DISORDER, LOCALIZATION AND DECAY IN QUANTUM WALKS

by

TENG JIAN KHOO

Frederick W. Strauch, Advisor

A thesis submitted in partial fulfillment
of the requirements for the
Degree of Bachelor of Arts with Honors
in Physics

WILLIAMS COLLEGE
Williamstown, Massachusetts

Contents

1 Introduction **2**
- 1.1 The Classical Walk and Markov Chains . . . 3
- 1.2 The Quantum Walk . . . 5
- 1.3 The Glued Trees Graph . . . 8
- 1.4 Imperfect walks . . . 10
- 1.5 Overview of results and conclusions . . . 12

2 Quantum walks on the Glued Trees Graph **15**
- 2.1 Motivations . . . 15
- 2.2 Definitions and characteristics . . . 16
- 2.3 Analyzing the Glued Trees graph: The column space . . . 18
- 2.4 Quantum Walk Propagation . . . 21
- 2.5 The full Glued Trees spectrum . . . 28
- 2.6 Discussion . . . 29

3 Disorder, Localization and Decay **32**
- 3.1 Motivations . . . 32
- 3.2 Fundamental concepts . . . 32
- 3.3 Decay from the column space . . . 35
- 3.4 Models of decay . . . 37
- 3.5 Discussion . . . 50

4 Simulations and results **51**
- 4.1 Numerical methods . . . 51
- 4.2 Numerical results . . . 53
  - 4.2.1 Ideal evolution . . . 54
  - 4.2.2 Disordered Evolution I: Column space decay . . . 56
  - 4.2.3 Disordered Evolution II: A quantum-to-classical Transition? . . . 60
  - 4.2.4 Disordered Evolution III: Whither localization? . . . 63
- 4.3 Discussion . . . 68

5 Conclusions **70**

1 Introduction

The classical random walk is a model with a substantial pedigree, and has provided insights to many problems in physics, including Brownian motion and diffusion. Its usefulness extends to numerous other fields of study. Examples thereof include ecology, in which random walks have been used to study foraging behavior [Zal07] and computer science, where random walks form the basis of various algorithms. Of particular interest is Papadimitriou's demonstration that a simple random walk model can solve the SAT problem with 2 variables with probability arbitrarily close to 1 in quadratic time, $\mathcal{O}(n^2)$; much faster than a brute-force search, which is exponentially slow, $\mathcal{O}(2^n)$ [Pap91]. The 3-SAT problem is NP-complete, and therefore it is of great interest to computer scientists that random walk algorithms accelerate the solution of SAT problems in general.

Like any good classical system, the random walk can be expressed in a quantum mechanical form, and the resulting 'quantum walk' exhibits novel and sometimes counterintuitive behavior. A thorough introduction to the subject is provided by Julia Kempe [Kem03]. Motivation for studying the quantum walk stems not only from the subject's intrinsic interest, but also from potential applications in quantum computation [Amb03]. Like the classical walk, the quantum walk has been found useful in the field of algorithms, and frequently demonstrates a speedup over the classical variety. A case in point is the field of quantum searches, such as those devised by Childs and Goldstone [CG04] and Shenvi et al. [SKW03]. The Shenvi algorithm is related to the Grover search [Gro96], which already demonstrates a quadratic quantum speedup.

A particularly striking case of the quantum speedup was demonstrated by Childs et al [CCD$^+$03]. They found that on a variant of the 'glued binary trees' graph, a quantum walker beginning at one of the roots could find the opposite root exponentially faster than any classical algorithm. However, the feasibility of exploiting this exponential speedup has been challenged. A recent paper [KLMW07] suggests that the imprecisions that an implementation of the computation would introduce might have devastating consequences on the evolution of the walk. Specifically, they claim that the phenomenon of Anderson localization [And58] leads to exponential suppression in the distance travelled by a quantum walk, a major hindrance to experimental realization.

In this thesis, we have undertaken a new analysis of the Glued Trees quantum walk. Using perturbation theory, we have devised a new model for the disordered walk, which agrees well with numerical simulations of the

exact case. These findings indicate that the effects of disorder are more complex than the simple localization effects found by Keating et al.

1.1 The Classical Walk and Markov Chains

> *The lesson of Lord Rayleigh's solution is that in open country the most probable place to find a drunken man who is at all capable of keeping on his feet is somewhere near his starting point!*
>
> Karl Pearson, 1905

The term 'random walk' first appears in a *Nature* letter from 1905, in which Karl Pearson requested a solution to the so-called 'drunkard's walk' in 2D: [Pea05]

> A man starts from a point O and walks l yards in a straight line; he then turns through any angle whatever and walks another l yards in a second straight line. He repeats this process n times. I require the probability that after these n stretches he is at a distance between r and $r + dr$ from his starting point, O.

The Gaussian large-n solution to Pearson's problem,

$$p_n(r < x < r + dr) = 2/n \, e^{-r^2/n} \, r \, dr, \tag{1.1}$$

was provided by Lord Rayleigh. The variance of the walker's position is linear in n. Even this early example illustrates the ubiquity of the random walk, as Rayleigh's original solution addressed the problem of monochromatic wave sources with randomized phases [Ray05].

The random walk on the line is a simpler binomial process, with a 'coin flip' at each time-step deciding whether the walker steps right or left. Hence, the position of the particle on the line is given by the binomial distribution, which in the large n limit approaches the normal distribution, assuming a fair coin toss (see Fig. 1). The variance once again spreads linearly in n.

For a more general description of a random walk on any graph, we can describe the probability distribution on the graph by a normalized vector $\vec{p}(t)$, with entries corresponding to the probability of being at each vertex. Let V designate the set of vertices of the graph, and the matrix M be a left stochastic $|V| \times |V|$ matrix where $M_{i,j}$ is the probability of stepping from vertex j to vertex i. Then, M is the transformation matrix for a single time-step,

$$\vec{p}(t + 1) = M \, \vec{p}(t), \tag{1.2}$$

Table 1: Probability distribution for the classical walk on the line

time-step, n	Position								
	-4	-3	-2	-1	0	1	2	3	4
0	0	0	0	0	1	0	0	0	0
1	0	0	0	1/2	0	1/2	0	0	0
2	0	0	1/4	0	1/2	0	1/4	0	0
3	0	1/8	0	3/8	0	3/8	0	1/4	0
4	1/16	0	4/16	0	6/16	0	4/16	0	1/16

and the time evolution of the system is given by

$$\vec{p}(t) = M^t \, \vec{p}(0). \tag{1.3}$$

This dynamics can be extended to cover continuous times as well. We will concern ourselves only with walks on undirected graphs, with unbiased coin flips. In this case, the discrete time transformation matrix is given by:

$$M_{i,j} = \begin{cases} 1/d_j, & i \neq j \text{ and } i \text{ and } j \text{ connected} \\ 0, & \text{otherwise} \end{cases} \tag{1.4}$$

Here, d_j denotes the degree of the vertex j, i.e. the number of sites connected to j. To fill in the probabilities for intermediate times, we first define the time step Δt, and the unit time hopping probability, i.e. the average probability of having made a transition, γ. At each vertex j, the likelihood of taking a transition is given by $\gamma_j = \gamma \, d_j$. Let Γ be the diagonal matrix, $\Gamma_{i,j} = \delta_{i,j} \, \gamma_j$. We then have the relation:

$$\vec{p}(t + \Delta t) \quad = \quad M(\Gamma \, \Delta t) \, \vec{p}(t) + (1 - \Gamma \, \Delta t) \, \vec{p}(t),$$

and thus

$$\begin{aligned} \frac{\vec{p}(t + \Delta t) - \vec{p}(t)}{\Delta t} &= M \, \Gamma \, \vec{p}(t) - \Gamma \, \vec{p}(t) \\ &= (M - \mathcal{I}) \, \Gamma \, \vec{p}(t) \quad = \quad -H \, \vec{p}(t), \end{aligned}$$

where we have defined the infinitesimal generator matrix $H = (\mathcal{I} - M)\Gamma$, whose matrix elements are given by

$$H_{i,j} = \begin{cases} d_i \, \gamma, & i = j \\ -\gamma, & i \neq j \text{ and } i \text{ and } j \text{ connected} \\ 0, & \text{otherwise} \end{cases} \tag{1.5}$$

Finally, letting the left hand side of this equation become the derivative (in the limit as Δt goes to zero), we see that the time evolution of the probabilities on the graph is determined by the master equation

$$\frac{d}{dt}\vec{p}(t) = -H\,\vec{p}(t), \tag{1.6}$$

where p_i and p_j represent the probabilities of being at vertices i and j respectively. Hence, we have a solution for the probability distribution on the graph, analogous to Eq. 1.3, of the form

$$\vec{p}(t) = \exp(-Ht)\,\vec{p}(0). \tag{1.7}$$

The matrix exponential is defined by its power series, analogously to the exponential of a number. However, the large number of terms involved typically makes calculation of the matrix exponential inefficient to compute. With this last equation we have established the classical picture of the random walk, so our next step will be to extend the concept of the random walk to the quantum regime.

1.2 The Quantum Walk

References to the notion of a quantum walk show up as early as 1946, in Feynman's path-integral derivation of the Dirac equation [Sch86]. However, the name was not coined until Aharonov, Davidovich and Zagury introduced their model of the 'discrete time quantum walk' in 1993 [ADZ93]. This model extends the idea of a coin flip to a measurement of some quantum system.

The Discrete Time Quantum Walk (DTQW)

The probabilistic nature of the classical coin flip can be modeled by measuring the state of a qubit in some basis $\{|\,0\,\rangle, |\,1\,\rangle\}$. The result of the measurement then determines which way the particle steps. As an example, consider once more the walk on the line. Define the two Hilbert spaces $\mathscr{H}_P$ and $\mathscr{H}_C$, corresponding to the location of the particle and the state of the coin, respectively. The former is an infinite-dimensional space spanned by the position states $\{|\,n\,\rangle \,|\, n \in \mathbb{Z}\}$, whereas the latter is a two-dimensional space spanned by the coin states $|\,0\,\rangle$ and $|\,1\,\rangle$.

We can implement a step of the walk by defining a conditional translation operator $S : \mathscr{H}_C \otimes \mathscr{H}_P \mapsto \mathscr{H}_C \otimes \mathscr{H}_P$. Specifically,

$$S = |\,0\,\rangle\langle\,0\,| \otimes S_L + |\,1\,\rangle\langle\,1\,| \otimes S_R, \qquad (S_{L,R} : \mathscr{H}_P \mapsto \mathscr{H}_P) \tag{1.8}$$

where S_L and S_R apply translations one step left or right respectively. Note that to apply the operator S, it is insufficient to only consider the position space of the walker – we must keep track of the coin state as well. So, we write the state of the walker as $|\,\psi\,\rangle = |\,c\,\rangle \otimes |\,x\,\rangle$[1], and thus the operator S acts as follows:

$$\begin{aligned} S|\,\psi\,\rangle &= S(|\,c\,\rangle \otimes |\,x\,\rangle) \\ &= \langle\,0\,|\,c\,\rangle(|\,0\,\rangle \otimes |\,x-1\,\rangle) + \langle\,1\,|\,c\,\rangle(|\,1\,\rangle \otimes |\,x+1\,\rangle). \end{aligned}$$

To simulate the random aspect of the walk, we must of course implement a coin flip as well. This is done by defining a unitary coin operator $C : \mathscr{H}_C \mapsto \mathscr{H}_C$. Various choices of the coin operator are possible, but typically we wish the operator to be fair, i.e. non-biased. That is, given a coin in either basis state, we would like the operator to take the coin state to an even superposition over the basis states. With such an operator defined, we can fully describe a step of the walk in the form

$$|\,\psi(t+1)\,\rangle = T|\,\psi(t)\,\rangle = S(C \otimes \mathcal{I}_P)|\,\psi(t)\,\rangle, \tag{1.9}$$

with $\mathcal{I}_P$ denoting the identity operator on the position space. One example of a balanced coin operator is given by the Hadamard coin,

$$C_H = \frac{1}{\sqrt{2}}\begin{pmatrix} 1 & 1 \\ 1 & -1 \end{pmatrix}. \tag{1.10}$$

At this point, we could recover the classical walk dynamics by measuring the coin's state at each time step and then applying T. Of greater interest is what occurs when we allow the system to evolve for some time *without* making any measurements, i.e. according to the equation

$$|\,\psi(t)\,\rangle = T^t|\,\psi(0)\,\rangle. \tag{1.11}$$

Then, the dynamics takes on uniquely quantum mechanical features. Whereas the classical walk results in the spreading of probabilities across the graph, the quantum walk leads instead to propagation of probability *amplitudes*.

Due to interference of probability amplitudes, quantum walk probability distributions look markedly different from the analogous classical distributions. For the Hadamard coin defined above, the quantum probability distribution is strongly peaked at the outer edges of the distribution, in

[1]Note: $|\,c\,\rangle \in \mathscr{H}_C$, and $|\,x\,\rangle \in \mathscr{H}_P$. The notation assumes that $|\,x\,\rangle$ is a state of definite position, but in general, $|\,x\,\rangle$ can be a superposition over multiple positions.

Table 2: Probabilities for the symmetric quantum walk on the line

time-step, t	Position								
	-4	-3	-2	-1	0	1	2	3	4
0	0	0	0	0	1	0	0	0	0
1	0	0	0	1/2	0	1/2	0	0	0
2	0	0	1/4	0	1/2	0	1/4	0	0
3	0	1/8	0	3/8	0	3/8	0	1/4	0
4	1/16	0	**6/16**	0	**2/16**	0	**6/16**	0	1/16

contrast with the classical Gaussian distribution. The quantum walk hence spreads quadratically faster than the classical walk – the standard deviation, $\sigma_{QW} \propto t$, while in the classical case, $\sigma_{CW} \propto \sqrt{t}$. In other words, quantum walks demonstrate ballistic propagation, rather than diffusive spreading.

Table 2 demonstrates the distinctions between the probability distributions of the classical and quantum walks. The probabilities presented are for a walk on the line, starting at position 0, with the symmetric coin state $1/\sqrt{2}(|\,0\,\rangle + i\,|\,1\,\rangle) \otimes |\,0\,\rangle$. The walk is evolved using the Hadamard coin (see Eq. 1.10) for four time steps, after which we already see the characteristic double-peaks of the quantum walk. Numbers in boldface are different from the classical walk distribution (compare with Table 1). The discrepancy becomes substantial at long times, as demonstrated in Fig. 1.

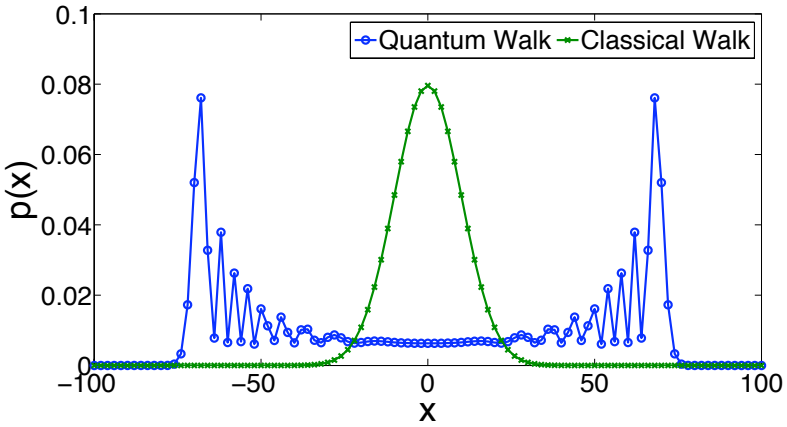

Figure 1: Comparison between the classical and quantum walks on the line after 100 time steps. The quantum walk is evolved using the Hadamard coin (Eq. 1.10), starting in the state $1/\sqrt{2}(|\,0\,\rangle + i|\,1\,\rangle) \otimes |\,0\,\rangle$.

The Continuous Time Quantum Walk (CTQW)

While the DTQW is an intuitive way of beginning to think about quantum walks, there is another model of the quantum walk, analogous to (classical) continuous time Markov processes [FG98]. The continuous time quantum walk drops the coin space, with the evolution of the wave-function instead being governed by a Hamiltonian derived from the adjacency matrix of the graph. Recall that the classical continuous time walk obeys (Eq. 1.6):

$$\frac{d}{dt}\vec{p}(t) = -H\,\vec{p}(t).$$

The conversion to the CTQW is as simple as converting the master equation above into a Schrödinger equation for the position of the particle. What was formerly the generator matrix H becomes the matrix Hamiltonian $\mathcal{H}$, and in the position space, the Schrödinger equation takes the form

$$\frac{d}{dt}|\,\psi(t)\,\rangle = -i\,\mathcal{H}\;|\,\psi(t)\,\rangle, \tag{1.12}$$

and the time evolution can be found by exponentiating the Hamiltonian,

$$|\,\psi(t)\,\rangle = e^{-i\,\mathcal{H}\,t}\,|\,\psi(0)\,\rangle. \tag{1.13}$$

Similar dynamics to the DTQW arise in the CTQW model, although there are some interesting distinctions. Some insights into the connections between the discrete- and continuous-time walks are provided by Strauch [Str06] and Childs [Chi08]. In general, the CTQW achieves similar speedups to the DTQW. However, these speedups are not sensitive to the coin, whereas the DTQW often shows vastly different results for different coin operators.

1.3 The Glued Trees Graph

Early motivations for studying the CTQW model were based on decision problems, which are easily represented in terms of decision trees. On such graphs, classical algorithms can be devised that efficiently negotiate the graph (e.g. the time to find the root node might be polynomial in the depth of the tree). Childs, Farhi and Gutmann devised a variant graph on which the quantum walk finds an 'EXIT' node exponentially faster than any classical algorithm. Specifically, they consider the graph of 'glued binary trees' G_d, constructed by identifying the leaves of two depth d binary trees, as depicted in Fig. 2 [CFG02].

The system is initally localized at the root of one of the trees (a.k.a. the entrance node; #1 in the figure) and the goal is to find the opposite

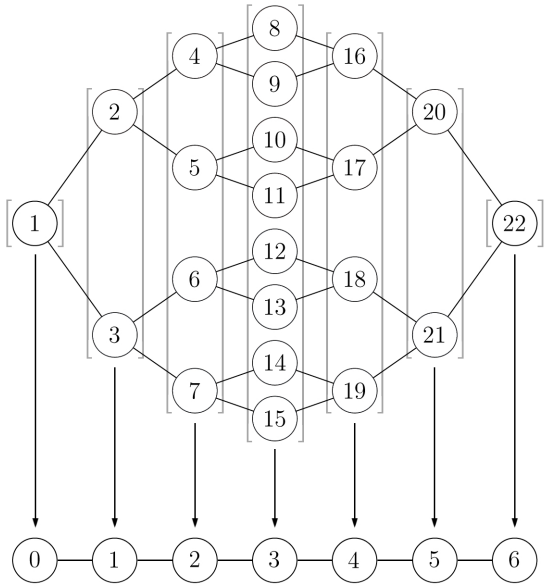

Figure 2: The graph G_d is reducible to a line of length $2d+1$, with the case $d = 3$ shown here.

(exit) root (#22 in the figure). Childs et al. showed that a quantum walk would traverse the graph exponentially faster than a classical random walk. Furthermore, they constructed an oracle problem, adding a random cycle on the leaves of the tree, such that a quantum walk-based algorithm finds the end exponentially faster than any classical algorithm [CCD$^+$03]. The cycle is a complication that we will disregard in this work.

The fast quantum traversal of the glued trees (GT) graph is due to the particular symmetry of the graph, which it shares with certain other graphs, such as the hypercube. When a walker starts localized at one of the roots of the tree, its propagation is confined to a subspace of the graph – the 'column space' (see Fig. 2). The states of the walker are restricted to evenly weighted superpositions over the states in each column of the graph, e.g.

$$|\,\mathrm{col}\;3\,\rangle = \frac{1}{\sqrt{8}} \sum_{i=8}^{15} |\,i\,\rangle.$$

This situation considerably simplifies analysis of the graph; rather than keeping track of the amplitude and phase of the system at each vertex of the graph, it is sufficient to do so for each column of the graph, effectively reducing the state evolution to a walk on the finite line.

It is fairly straightforward to calculate the size of the Hilbert space for the GT graph. Utilizing the mirror-symmetry of the graph, we note that identifying the leaves of the two binary trees ensures that length of the graph (the number of columns) is odd. Specifically, a GT graph of depth d has length $l = 2d + 1$, since a single binary tree has $d + 1$ columns, and the second contributes only d additional columns. Considering only the left tree, we see that the jth column contains 2^j vertices, where we begin numbering from $j = 0$ (see Fig. 2). Hence, the central column has 2^d vertices, while the remainder of the columns to the left have $2^d - 1$, as can be seen from Fig. 2.[2] The same applies to the columns on the right of the center. Therefore, we see that the total number of vertices on the graph is $N_d = 3(2^d) - 2$. By similar arguments, we can count the number of edges of the graph. Proceeding inwards from the two roots, we see that each vertex is connected to two edges leading inwards. We run out of edges one column from the center on either side. Thus, we have the number of edges, $N_e = 2(N_d - 2^d) = 4(2^d - 1)$.

The column states form an orthonormal basis for an l-dimensional subspace of the graph's N_d-dimensional Hilbert space. Due to the symmetries discussed earlier, the walk remains restricted to the column space for all time. Since, with the exception of the first and last, each column space state is connected only to the two adjacent column space states (e.g. $|\,\text{col } 3\,\rangle$ couples only to $|\,\text{col } 2\,\rangle$ and $|\,\text{col } 4\,\rangle$), we see that the graph structure is congruent to a finite line.

As previously discussed, the continuous time walk on the line propagates at a constant speed, and therefore the hitting time, i.e. the time needed for a walker to proceed from the start node to the end node with substantial probability, is also linear in the length of the graph. On the other hand, a classical walker is expected to only have an exponentially small probability of being at the end node at all times. Hence, we conclude that the quantum walk on the GT graph is exponentially faster than the classical walk.

1.4 Imperfect walks

If we are ever to put quantum walks to use (or indeed if they are actualized anywhere in nature), imperfections must inevitably surface in their implementation. Specifically, we would expect to see noise in the form of decoherence and disorder affecting the quantum walk. Decoherence involves unwanted couplings, such as to the environment, that cause loss of information, rendering the walk's evolution nonunitary. For more information

[2] Alternatively, because $\sum_{j=0}^{d-1} 2^j = 2^d - 1$.

on decoherent quantum walks, see Kendon's review [Ken07]. We primarily concern ourselves with noise in the form of disorder.

Whereas decoherence refers to a distortion of the walk's evolution, such as the action of imperfect operators, or random measurements in which information is lost, disorder is characterized by variations in the structure of the Hamiltonian away from the ideal. For the purposes of this thesis, we will restrict the discussion to static disorder. In an experimental setting, static disorder might be introduced by our inability to perfectly set up the Hamiltonian, resulting in uneven site energies or bond lengths.

Mathematically, static disorder can be represented by adding small error terms to the Hamiltonian:

$$\mathcal{H} = \mathcal{H}_0 + \mathcal{H}_s + \mathcal{H}_b = \mathcal{H}_0 + \sum_i \epsilon_i |\, i \,\rangle\langle\, i \,| + \sum_{\substack{i,\,j \\ i \neq j}} \epsilon_{i,j}\, \mathcal{H}_{i,\,j} \,|\, i \,\rangle\langle\, j \,|, \tag{1.14}$$

with $\mathcal{H}_0$, $\mathcal{H}_s$ and $\mathcal{H}_b$ representing the ideal, site disorder, and bond disorder Hamiltonians, respectively. The result is that the eigenstates of the system are perturbed, with corresponding energy shifts and additional couplings. This causes the evolution of the system to be disrupted, although in a manner that is in principle predictable. That is, for an individual instance of disorder, the system's evolution remains unitary, i.e. obeys a Schrödinger equation. However, we typically do not know the disorder terms exactly, and so might only be able to determine the evolution averaged over many realizations of $\mathcal{H}$. This could be construed as a form of information loss.

In the case of quantum walks, disorder changes the relative phases of the walk along different paths, and hence the normal interference effects are modified. Typically, this hinders the walk propagation. Keating et al. have recently suggested that static disorder on the Glued Trees graph might result in Anderson localization, a phenomenon well-studied in solid-state physics, in which the system eigenstates become exponentially localized. [KLMW07]. This localization would lead to an exponential suppression of the propagation of the walk, substantially hindering any attempts at quantum walk-based computation.

Keating's paper analyzed the results of static site disorder in the column space, introducing small error times on the diagonal of the column space Hamiltonian. This produces a perturbed Hamiltonian

$$\mathcal{H}_{\text{col}}{}' = \mathcal{H}_{\text{col}} + \sum_{j=0}^{2d} \epsilon_j |\, \text{col}\; j \,\rangle\langle\, \text{col}\; j \,|. \tag{1.15}$$

Simulations of the disordered walks resulted in apparent exponential localization, in keeping with the predictions of Anderson localization. More disturbing, they suggest that a quantum walker could be trapped at the entrance node, not even reaching the graph's center, and thus performing worse than the classical walker.

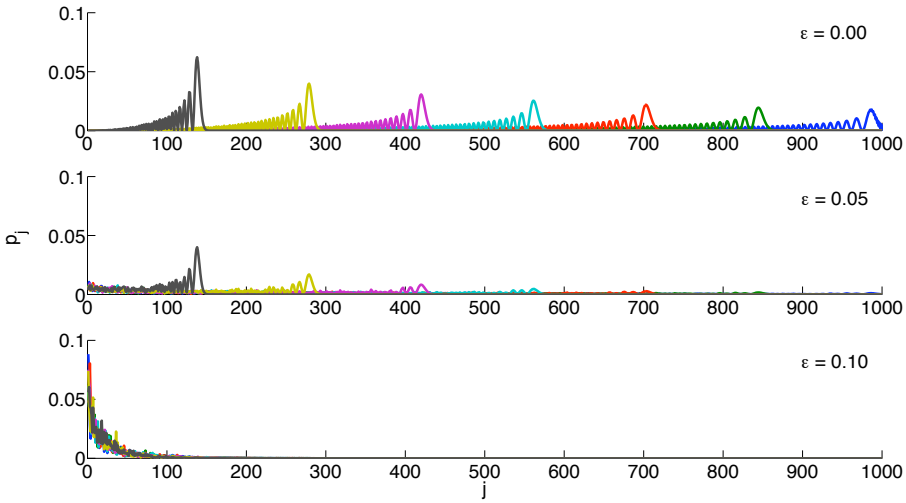

Figure 3: Disorder-induced exponential localization. The plots are of p_j, the probability of being at column-state j, with time t growing in increments of $t = 50$.

Although the numerical evidence for localization appears compelling, it may not be sufficient to assume that the column space simulations fully describe the behavior of quantum walks on the Glued Trees graphs. Specifically, it is known that Anderson localization is inevitable in one-dimensional disordered systems, but not in multi-dimensional systems [Bor63, AALR79]. There is hence room for optimism: the GT graph has higher-dimensional structure that might allow a greater degree of propagation.

1.5 Overview of results and conclusions

This thesis examines the Glued Trees graphs in the hopes of understanding the detrimental effects of disorder on quantum walk propagation. We first derive several known analytical results in the dynamics of the walk. In addition, we define a new diagnostic of the walk propagation, specifically

the average depth d_{avg}, leading to some extra insights about the nature of the walk. This analysis is extended to the disordered dynamics using perturbation theory, culminating in the creation of a dynamical model of the walk in the one-dimensional column space that closely captures the characteristics of the multi-dimensional disordered walk.

Our preliminary goal was to derive a mapping, if one could be found, between the vertex-space Hamiltonian $\mathcal{H}$, Eq. 1.14 and a column space Hamiltonian such as that in Eq. 1.15, which would allow for efficient simulation of the quantum walk. However, due to the one-dimensional nature of $\mathcal{H}_{\text{col}}$, the disordered dynamics are dominated by Anderson localization, which sets in for small values of disorder ($\varepsilon \sim 0.5$). In contrast, the vertex-space simulations demonstrate that the linear propagation of the quantum walk is retained for weak disorder ($\varepsilon \lesssim 1.0$), although there is a turnover from quantum to classical behavior. To describe this transition to classical propagation, we find it necessary to account for the expanded dynamics of the walk that take place outside the column space.

The advantages of the quantum walk over the classical on the Glued Trees result from the coherent quantum transport in the column space of the graph. As disorder opens up the possibility of the walk escaping from this subspace of the graph, we treat the column space as a decaying quantum system, coupled to a large space by the disorder perturbation. Using results from first-order perturbation theory and Fermi's Golden Rule, we develop a simple dynamical model to account for the column space decay: the *local decay model*, computed in the column space. Essentially, we propose that an appropriate column space mapping is given by the *non-unitary* prescription:

$$\mathcal{H} \quad \mapsto \quad \mathcal{H}_{\text{col}} - i\Gamma_j/2, \tag{1.16}$$

where the column-dependent decay rate,

$$\Gamma_j = \frac{\sigma^2}{\gamma}(1 - {N_j}^{-1}). \tag{1.17}$$

In the decay rate Γ_j, we write σ^2 for the variance of the error terms, $\langle \epsilon^2 \rangle$, and γ for the coupling strength. This model allows us to determine the column space probability p_{col} and the hitting probability p_{hit} at the opposite root from the starting point for times up to twice the first hitting time, in the weak disorder regime.

Because of the column space decay, the hitting probability suffers a reduction that is exponential in the variance of the disorder strength σ^2 and the depth of the graph d. This is similar to the prediction from localization

theory, although quantitatively it is less severe, allowing substantial propagation for small amounts of disorder. The mechanism for the reduction is, however, quite different. As the strength of disorder is increased, a localization transition is reached, beyond which the quantum walk no longer propagates freely. It instead becomes trapped at the starting point, in agreement with analyses of localization on the infinite Cayley tree [ACTA73, JG79].

The remainder of this thesis is organized as follows: We first analyze the Glued Trees walks in depth, taking the ideal Hamiltonian and deriving the spectrum of the graph, from which we can determine expected behavior such as the hitting time, and the probability of being at any vertex, or in the column space at a given time. We then address the question of disordered walk dynamics, using perturbation theory and Fermi's Golden Rule to devise the local decay model mentioned above. Finally, we compare the results of our model with simulations of the vertex-space Hamiltonian.

Ultimately, we hope that the insights gained regarding disorder and decay on the Glued Trees graphs can be extended to systems with similar properties. In particular, other graphs that share the symmetries that allow representation in the column space should benefit from the analysis of column space decay, and the construction of analogous local decay models. Additionally, we have uncovered more connections between dimensionality and disorder's effects.

In terms of robustness against disorder, our findings indicate that the Glued Trees graph lie between the line and the hypercube, the former succumbing to localization for arbitrarily small disorder, while the latter retains propagation far longer. This difference in robustness reflects a strong dependence on the dimensionality and degree of the graphs. There is something of a competition at work, in that the large (geometric) dimensionality of the GT graph works against localization, but at the same time, it contributes to the proliferation of non-column space states which allow the column space decay to take place.

2 Quantum walks on the Glued Trees Graph

2.1 Motivations

> *To view the Church-Turing hypothesis as a physical principle does not merely make computer science a branch of physics. It also makes part of experimental physics into a branch of computer science.*
>
> David Deutsch, 1985

In this study of quantum walks and disorder, we will primarily be concerned with the dynamics on the class of graphs known as the Glued (Binary) Trees. Conceptually simple to describe, this set of graphs nevertheless plays host to a variety of interesting phenomena in the context of quantum walks. As they are related to decision trees, the graphs are also of considerable interest from the standpoint of computer science, and quantum computation.

Of central importance to computer science, and in particular the study of computational complexity, is the dichotomy between polynomial and exponential. A computer scientist's Holy Grail is a proof of the equality or inequality of the computational complexity classes P and NP, the former containing all problems soluble in polynomial time, and the latter containing all problems whose solutions can be verified in polynomial time. The class NP turns out to be equivalent to the set of problems which can be solved in polynomial time by a *nondeterministic* computer, i.e. one that explores all computational paths simultaneously.

The celebrated Cook-Levin theorem [Coo71, Lev73] states that the Boolean satisfiability problem (SAT) is *NP-complete*, which is to say that any problem in NP can be reduced to an instance of SAT with only polynomial slowdown. Specifically, a problem in SAT takes the form of a Boolean formula (binary variables linked by the logical operators AND, NOT and OR), and the goal is to determine whether an assignment of TRUE/FALSE values to the variables can result in the formula evaluating to true. The theorem then allows for any problem in NP to be expressed in the form of such a formula, so if an algorithm can be devised to efficiently (read: in polynomial time) solve SAT, then it will likewise efficiently solve every problem in NP, proving $P = NP$.

What relevance, if any, has this to quantum mechanics? Well, ever since the advent of Deutsch's quantum algorithm, which demonstrated a factor of 2 speedup over *any* classical algorithm on an admittedly artificial

problem [Deutsch '85], interest in quantum algorithms has ballooned, offering up numerous quantum mechanical algorithms that outdo their classical counterparts by quadratic, and even exponential speedups. While quantum computers are 'disqualified' from competing in P versus NP, they still offer hope of relatively efficient solutions to hard computational problems.

As alluded to previously, Papadimitriou showed in 1991 that random walks offer an efficient probabilistic strategy to solve SAT. In 1997, inspired directly by similar uses of random walks in computer science, Farhi and Gutmann introduced the Continuous Time Quantum Walk, comparing the propagation of a quantum walker versus a classical walker on decision trees [FG98]. They found that on such decision trees, the quantum walker's penetration of the graph was exponentially faster than the classical walker's. A further triumph was demonstrated in 2002, when Childs et al. proved that a quantum walker crossed the Glued Trees graph (with a random permutation on the leaves) exponentially faster than any classical algorithm whatsoever [CFG02]. An advantage of studying the GT graph, as opposed to its progenitor decision trees, is that the graph structure leads to a simplified Hamiltonian. In addition, the isolation of a single target state (the exit node) gives a simple criterion for success.

In this section, we will present more thoroughly the mathematical structure of quantum walks on the GT graphs. Then, we will derive several characteristics of the GT walks, contrasting them with the classical results.

2.2 Definitions and characteristics

As mentioned earlier, the GT graph of depth d (see Fig. 4) is formed by constructing two binary trees of depth d (i.e. with 2^d leaves), and identifying the leaves of the two trees. It contains $N_d = 3(2^d) - 2$ vertices, connected by $N_e = 4(2^d - 1)$ edges. Hence, the number of vertices, and correspondingly the size of the Hilbert space needed to represent the graph, grows exponentially in the depth. The exponential size is a substantial obstacle when it comes to computing the matrix exponentiation.

A natural organization of the GT graph is to group the vertices into columns, based on their distance (the number of links in the shortest path) from the roots of the graph. Picking one root arbitrarily (the left root/start node), there will be 2^j vertices at distance j from the root, until we reach the center, which contains 2^d vertices. From there onwards, the graph is mirrored, so we have instead 2^{l-j} vertices at distance j, where we have defined the length of the graph, $l = 2d + 1$, which is equal to the number of columns in the graph.

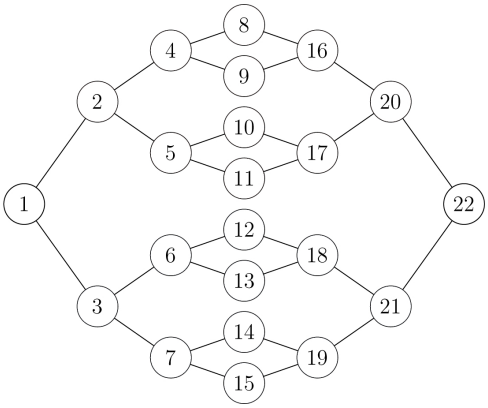

Figure 4: The $d = 3$ Glued Trees Graph

We adopt the convention of labeling the graph vertices integers i in the range $1 \leq i \leq N_d$, calling the left root $i = 1$ and proceeding as illustrated in Fig. 4. The columns of the graph are similarly labeled by integers j, but with the range $0 \leq j \leq 2d$. This labelling has the nice feature that the 'topmost' vertex in column j has label $i = 2^j$, for columns 0 to d. By the mirror symmetry of the graph, a similar structure holds for the remaining columns, whereby the 'bottom' vertex in each column has $i = N_d + 1 - 2^{l-j}$.

The problem established by Childs et al. is to start at the left root, and cross the graph to reach the opposite root [CFG02]. An equivalent formulation is to find the instantaneous (one-shot) hitting probability,

$$p_{hit}(t) \;=\; |\langle\, \psi_{end} \,|\, U(t) \,|\, \psi_{start} \,\rangle|^2 \;=\; |\langle\, N_d \,|\, U(t) \,|\, 1 \,\rangle|^2 \tag{2.1}$$

between the start and end nodes, with $U(t)$ standing for the time evolution operator.[3] It turns out that a classical walker is very good at proceeding halfway across the graph – but not further. Since every vertex has twice as many edges leading towards the center than outwards, picking edges at random is twice as likely to lead a walker to the central column of the graph. At long times, the classical random walk probabilities 'mix', i.e. asymptotically approach the uniform distribution over the vertices of the graph. So, we expect the hitting probability of a classical walker after a long time (and an upper bound on the hitting probability at any time) to be given by

$$p_{hit}(t \to \infty) \;\cong\; {N_d}^{-1} \;\cong\; \frac{1}{3}(2^{-d}). \tag{2.2}$$

[3]The hitting probability can in principle be defined for any pair of vertices. In this thesis, we are only interested in the end-to-end hitting probability, and define p_{hit} as such.

So we see that the classical walker's probability of reaching the end node at any individual time is exponentially small in the depth d of the graph G_d. The probability of ever having hit the exit node thus takes an exponentially long time to become substantial, i.e. the walker takes a long time to reach the exit. To show that the quantum walker outperforms the classical walker, in terms of a larger one-shot hitting probability and hence earlier arrival at the exit, we next introduce the concept of the column space.

2.3 Analyzing the Glued Trees graph: The column space

As the length $l = 2d+1$ of a given GT graph grows linearly with the depth d, computations in the column space are simplified dramatically as compared with the full vertex-space calculations, which involve $N_d = 3(2^d)-2$ vertices, and therefore an $N_d \times N_d$ Hamiltonian, denoted in the ideal case by $\mathcal{H}_0$. We denote the $l \times l$ column space Hamiltonian as $\mathcal{H}_{\text{col}}$. The states in the column space for the graph G_d are defined as follows:

$$|\,\text{col}\; j\,\rangle = \frac{1}{\sqrt{N_j}} \sum_{a\,\in\,\text{column}\,j} |\,a\,\rangle, \tag{2.3}$$

where we define

$$N_j = \begin{cases} 2^j, & 0 \le j \le d \\ 2^{2d-j}, & d < j \le 2d \end{cases} \tag{2.4}$$

and the vertex state $|\,a\,\rangle$ is in column j if

$$a \in \begin{cases} [N_j, 2N_j - 1], & 0 \le j \le d \\ N + 1 - [N_j, 2N_j - 1], & d < j \le 2d \end{cases} \tag{2.5}$$

As an illustration, consider the graph G_2, with depth $d = 2$. We have $N_d = 10$, $l = 5$. The Hamiltonian takes the form

$$\mathcal{H}_0 = -\gamma \begin{pmatrix} -2 & 1 & 1 & 0 & 0 & 0 & 0 & 0 & 0 & 0 \\ 1 & -3 & 0 & 1 & 1 & 0 & 0 & 0 & 0 & 0 \\ 1 & 0 & -3 & 0 & 0 & 1 & 1 & 0 & 0 & 0 \\ 0 & 1 & 0 & -2 & 0 & 0 & 0 & 1 & 0 & 0 \\ 0 & 1 & 0 & 0 & -2 & 0 & 0 & 1 & 0 & 0 \\ 0 & 0 & 1 & 0 & 0 & -2 & 0 & 0 & 1 & 0 \\ 0 & 0 & 1 & 0 & 0 & 0 & -2 & 0 & 1 & 0 \\ 0 & 0 & 0 & 1 & 1 & 0 & 0 & -3 & 0 & 1 \\ 0 & 0 & 0 & 0 & 0 & 1 & 1 & 0 & -3 & 1 \\ 0 & 0 & 0 & 0 & 0 & 0 & 0 & 1 & 1 & -2 \end{pmatrix}. \tag{2.6}$$

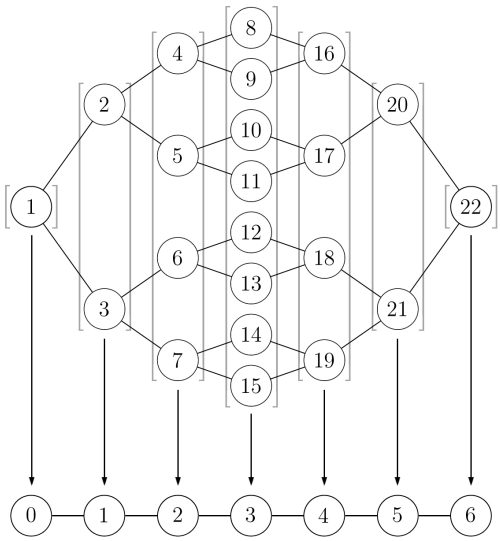

Figure 5: The graph G_3 is reducible to a line of length $2(3)+1$, via the mapping P. [Reproduced from Fig. 2]

To convert this to the column space Hamiltonian, we can apply the mapping

$$P = \sum_j |\,\tilde{\text{col}}\, j\,\rangle\langle\,\text{col}\, j\,|, \tag{2.7}$$

where $|\,\tilde{\text{col}}\, j\,\rangle$ denotes a single state on a line, representing the column state $|\,\text{col}\, j\,\rangle$. Thus, we define the column space Hamiltonian

$$\mathcal{H}_{\text{col}} \;=\; P\,\mathcal{H}_0\,P^\dagger \;=\; -\gamma \begin{pmatrix} -2 & \sqrt{2} & 0 & 0 & 0 \\ \sqrt{2} & -3 & \sqrt{2} & 0 & 0 \\ 0 & \sqrt{2} & -2 & \sqrt{2} & 0 \\ 0 & 0 & \sqrt{2} & -3 & \sqrt{2} \\ 0 & 0 & 0 & \sqrt{2} & -2 \end{pmatrix}. \tag{2.8}$$

The resulting Hamiltonian is typically simplified by disregarding the diagonal terms, as subtraction of a -2 from all the diagonal terms simply leads to an irrelevant energy shift, while in the large d limit, the defects at the ends and center of the graph do not significantly affect propagation. Unlike in the classical case, probability conservation is ensured by the Hermiticity of $\mathcal{H}$. Happily, this reduces our problem to a familiar one: $\mathcal{H}_{\text{col}}$ is of exactly

the same form as the matrix describing a set of l coupled oscillators:

$$\mathcal{H}_{\rm col} = -\sqrt{2}\,\gamma \begin{pmatrix} 0 & 1 & 0 & 0 & 0 \\ 1 & 0 & 1 & 0 & 0 \\ 0 & 1 & 0 & 1 & 0 \\ 0 & 0 & 1 & 0 & 1 \\ 0 & 0 & 0 & 1 & 0 \end{pmatrix}. \tag{2.9}$$

The eigenvalues are distributed as

$$E_{k,d} = 2\sqrt{2}\,\gamma\,\cos\!\left(\frac{k\,\pi}{2(d+1)}\right), \tag{2.10}$$

with corresponding eigenvectors

$$|\,\tilde{\Psi}_{k,d}\,\rangle = \frac{1}{\sqrt{d+1}} \sum_{j=0}^{2d} \sin\!\left(\frac{k\,(j+1)\,\pi}{2(d+1)}\right) |\,\tilde{\rm col}\;j\,\rangle, \tag{2.11}$$

where k takes integer values between 1 and $2d+1$ inclusive. We designate these the column space eigenvalues and eigenstates.[4] With these in hand, it is a straightforward task to diagonalize the Hamiltonian in the energy basis, at which point the dynamics of the system is known.

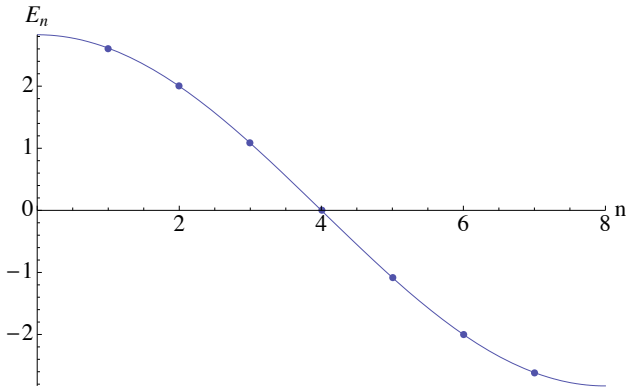

Figure 6: The column space eigenvalues of the graph G_3.

[4]Note that the definition here is on the line-reduced graph, but it is also valid for states on the full graph, which we would notate without the tildes.

2.4 Quantum Walk Propagation

Bessel Function Analysis: The Green's Function

To apply the results of our analysis to the specific problem we are considering, i.e. the root-to-root graph traversal, we should begin by finding the starting state $|\,\psi_{start}\,\rangle = |\,\tilde{\text{col}}\ 0\,\rangle$ in terms of the energy eigenstates. By Fourier's trick, the eigenstate decomposition is given by

$$|\,\psi_{start}\,\rangle \;=\; \sum_{k=1}^{2d+1} \langle\,\tilde{\Psi}_{k,d,}\,|\,\text{col}\,0\,\rangle|\,\tilde{\Psi}_{k,d,}\,\rangle \;=\; \sum_{k=1}^{2d+1} \frac{\sin\!\left(\frac{k\,\pi}{2(d+1)}\right)}{\sqrt{d+1}}|\,\tilde{\Psi}_{k,d}\,\rangle. \quad (2.12)$$

So, the wavefunction on the line-reduced graph has the form

$$|\,\psi(t)\,\rangle \quad = \quad \sum_{k=1}^{2d+1} \frac{\sin\!\left(\frac{k\,\pi}{2(d+1)}\right)}{\sqrt{d+1}}\, e^{-iE_{k,d}\,t}|\,\tilde{\Psi}_{k,d}\,\rangle. \quad (2.13)$$

For notational simplicity, we will henceforth drop the subscript d on the eigenvalues and eigenstates, and understand that the sum over k runs from 1 to $l = 2d + 1$. We thus have

$$\begin{aligned} |\,\psi(t)\,\rangle \quad &= \quad \sum_{k}\, e^{-iE_k\,t}\frac{\sin\!\left(\frac{k\,\pi}{2(d+1)}\right)}{\sqrt{d+1}}|\,\tilde{\Psi}_k\,\rangle \\ &= \quad \sum_{k,\,j}\, \frac{\sin\!\left(\frac{k\,\pi}{2(d+1)}\right)\,\sin\!\left(\frac{k\,(j+1)\,\pi}{2(d+1)}\right)}{\sqrt{d+1}}\, e^{-iE_k t}\,|\,\tilde{\text{col}}\ j\,\rangle. \end{aligned} \quad (2.14)$$

At this point, the state of the wavefunction is not difficult to evaluate at a given time t, but the form of the expression is not especially enlightening. We can glean more information by moving to a continuum limit. To do so, let $\theta = k\,\pi/2(d+1)$ and $\omega = 2\sqrt{2}\gamma$. We further convert the sum to an integral,

$$\frac{1}{d+1}\sum_{k}(\ldots) \quad \rightarrow \quad \frac{2}{\pi}\int(\ldots)\,d\theta.$$

Then, taking Eq. 2.14 and substituting in Eq. 2.10 for E_k, we have

$$|\,\psi(t)\,\rangle = \sum_{j}\, \frac{2}{\pi}\int_0^{\pi}\, \sin\theta\,\sin(j+1)\theta\, e^{-i\omega t\,\cos\theta}\,d\theta\,|\,\tilde{\text{col}}\ j\,\rangle. \quad (2.15)$$

Note that we have implicitly added two points to the wavefunction above, i.e. those at $\theta = 0,\,\pi$. This is fine – the eigenstates are zero there anyway.

Rearranging the sines into a difference of cosines,

$$\sin\theta\,\sin(j+1)\theta \quad = \quad \frac{1}{2}\big(\cos j\theta - \cos(j+2)\theta\big),$$

we obtain the expression

$$|\,\psi(t)\,\rangle = \sum_j \frac{2}{\pi}\int_0^\pi \frac{1}{2}\big(\cos j\theta - \cos(j+2)\theta\big)\,e^{-i\omega t\,\cos\theta}\,d\theta\,|\,\tilde{\text{col}}\;j\,\rangle. \quad (2.16)$$

This pair of integrals can be represented in terms of Bessel functions [AS65], up to a complex factor. The propagation of the walker is best expressed in terms of the Green's function G, i.e. the wavefunction's amplitude at site j,

$$\begin{aligned} G(0,\,j,\,t) &= \langle\,\tilde{\text{col}}\;j\,|e^{-i\,\mathcal{H}\,t}|\,\tilde{\text{col}}\;0\,\rangle \\ &= i^j\,(J_j(\omega t) + J_{j+2}(\omega t)) \\ &= i^j\,\frac{2j}{\omega t}J_{j+1}(\omega t). \end{aligned} \quad (2.17)$$

This Bessel function solution decays monotonically, whereas a wavepacket propagating on a finite line must be reflected by the edges, which means there must be recurrences of the probability not predicted by this model.[5]

The problem is resolved by assuming periodicity of the system (starting again in the discrete case), working on an infinite line instead of the line of length $l = 2d+1$, and letting the states $\{|\,\tilde{\text{col}}\;0\,\rangle, \ldots, |\,\tilde{\text{col}}\;l-1\,\rangle\}$ represent the original finite line. We will furthermore associate the state $|\,\tilde{\text{col}}\;l\,\rangle$ with this set of states. Additionally, we assume the eigenstates $|\,\tilde{\Psi}_1\,\rangle$ through $|\,\tilde{\Psi}_l\,\rangle$ remain the eigenstates of the system, but extend the domain of the sinusoidal functions to include states outside the original finite line. Finally, we impose the same initial conditions on the wavefunction:

$$|\,\psi_{start}\,\rangle \;=\; \sum_{k=1}^{d}\langle\,\tilde{\Psi}_{k,d,}\,|\,\tilde{\text{col}}\,0\,\rangle|\,\tilde{\Psi}_{k,d,}\,\rangle \;=\; \sum_{k=1}^{2d+1}\frac{\sin\!\left(\frac{k\,\pi}{2(d+1)}\right)}{\sqrt{d+1}}|\,\tilde{\Psi}_{k,d}\,\rangle. \quad (2.18)$$

Admittedly, this 'state' is not normalized, but the segment of it restricted to the range of column states $\{0, \ldots, l\}$ is.[6] The same applies for each chunk of the line, $\{\,|\,\tilde{\text{col}}\;(0+n(l+1))\,\rangle, \ldots, |\,\tilde{\text{col}}\;(l+n(l+1))\,\rangle\,\}$, where $n \in \mathbb{Z}$. Since the sine function is periodic, we know the amplitudes of $|\,\tilde{\text{col}}\;j\,\rangle$ and

[5] Of course, when we moved to the continuum limit, the range of possible j became infinite, so it should be no surprise that the wavefunction keeps traveling indefinitely.

[6] This is because the amplitude at $|\,\tilde{\text{col}}\;l\,\rangle$ is zero due to the choice of eigenstates

$|\,\tilde{\text{col}}\,(j+2n(l+1))\,\rangle$ to be equal, for $j \in \{0, \ldots, l\}$ and $n \in \mathbb{Z}^+$ and likewise for $|\,\tilde{\text{col}}\,(-j)\,\rangle$ and $|\,\tilde{\text{col}}\,j\,\rangle$ for $j \geq 0$.

If we now take the continuum limit and integrate, we have not just one Bessel function solution but infinitely many, offset from each other in time. Another way to think about the result is to imagine that, rather than a single source at $|\,\tilde{\text{col}}\,0\,\rangle$, we instead have an infinite number located at $|\,\tilde{\text{col}}\,(0 \pm 2n(l+1))\,\rangle$ for $n \in \mathbb{Z}$. The finite line Green's function G' becomes

$$\begin{aligned} G'(0,\, j,\, t) &= \langle\,\tilde{\text{col}}\,j\,|e^{-i\,\mathcal{H}\,t}|\,\tilde{\text{col}}\,0\,\rangle \\ &= \sum_{n=-\infty}^{\infty} G(0,\, j+2n(l+1),\, t), \end{aligned} \tag{2.19}$$

with G given by Eq. 2.17. So we see that the function G we found earlier is merely the first term in this series. This new expression gives perfect agreement with the exact amplitudes found by summing the time-evolved energy eigenstates $e^{iE_k t}|\,\tilde{\Psi}_k\,\rangle$ (See Fig. 7).

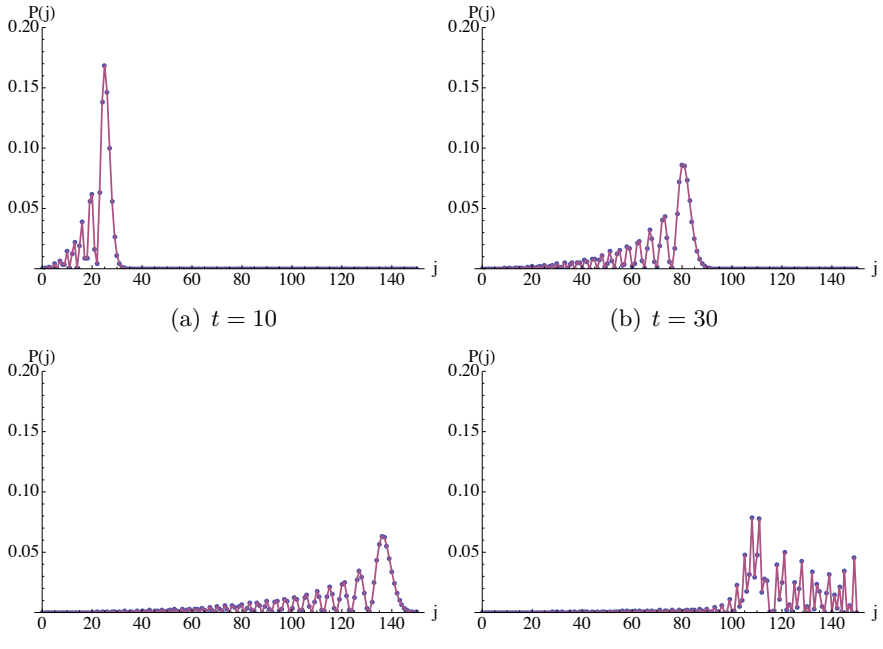

(a) $t = 10$ (b) $t = 30$

(c) $t = 50$ (d) $t = 70$

Figure 7: The quantum walk on the columns of G_{75}, showing the reflection from the right root. The points indicate the approximate Bessel function solutions, while the line is the exact solution from diagonalizing $\mathcal{H}_{\text{col}}$.

The Average Depth

The Bessel function analysis provides us with a nice local description of the quantum walk, in the sense that we know how the walk behaves at each site. However, it would also be enlightening to have some sort of global characterization. With that in mind, we wish to define an additional quantity, the average depth $d_{avg}(t)$ reached by the walker:

$$d_{avg}(t) = \langle\, \psi(t) \,|\, \hat{j} \,|\, \psi(t) \,\rangle, \tag{2.20}$$

where $\hat{j}$ is the column position operator, whose action on a column state is

$$\hat{j}|\, \tilde{\text{col}}\; j \,\rangle = j|\, \tilde{\text{col}}\; j \,\rangle.$$

We compute this using the column state basis, substituting in two copies of Eq 2.14. Each introduces a sum over the column states, which we index by k and k', so we need to compute a triple sum in j, k and k'. For brevity, we make the substitution $j' = j + 1$. The sum then has the form:

$$d_{avg}(t) = \sum_{k=1}^{l} \sum_{k'=1}^{l} f(k,\, k')\, e^{it(E_k - E_{k'})}, \tag{2.21}$$

where we have set, as before, $\theta = k\,\pi/2(d+1)$ and $\theta' = k'\,\pi/2(d+1)$. The function $f(k,\, k')$ is given by

$$f(k,\, k') = \sum_{j'=1}^{l} \frac{(j'-1)\sin(j'\theta)\,\sin(j'\theta')\,\sin(\theta)\,\sin(\theta')}{(d+1)^2}. \tag{2.22}$$

If we plot just the magnitude of f, corresponding to the coefficients of the exponentials, we see (Fig. 8) that the largest contributions come in three diagonal lines, i.e. with $k' = k$, and $k' = k \pm 1$. This suggests that a reasonable approximation might be found by keeping only these terms in the triple sum, which in fact turns into a double sum. Let us first find the sum of the $k = k'$ terms, which will be constant in time, denoting it f_0. In the integral approximation, where we treat θ as a continuous variable, we have:

$$f_0 = \sum_{j'=1}^{l} \frac{2(j'-1)}{\pi\,(d+1)} \int_0^{\pi} \sin^2\!\big(j'\theta\big)\,\sin^2(\theta)\; d\theta. \tag{2.23}$$

The integral is straightforward, and evaluates to $\pi/4$. The sum follows with as little fuss, to give $f_0 = d$. This is a reassuring result – since the walker has

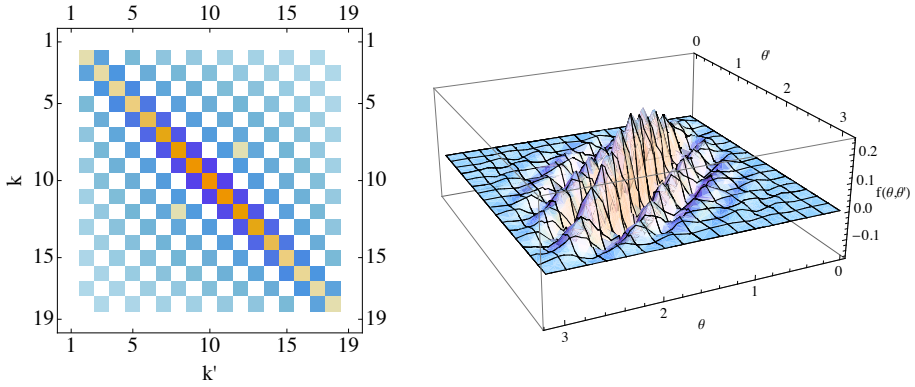

(a) The discrete coefficients, $f(k,\, k')$. Color intensity scales with amplitude.

(b) The continuum limit, $f(\theta,\, \theta')$.

Figure 8: Plots of the discrete and continuum limits of f, for $d = 11$

a tendency to stay in the middle of the graph, we would expect the constant term in d_{avg} to be d. A quick numerical check shows that the discrete sum over k in place of θ yields the same result. So we can move on to the case $k' = k \pm 1$.

Without loss of generality, we can take $\theta > \theta'$. We can furthermore combine the two sums, as they only differ in the sign of the complex exponential. This turns the exponential factor into a cosine,

$$e^{i\omega t(\cos\theta - \cos\theta')} + e^{-i\omega t(\cos\theta - \cos\theta')} = 2\cos\big(\omega t(\cos\theta - \cos\theta')\big)\,.$$

In the limit of large d, the difference $\Delta\theta = \theta - \theta' = \pi/2(d+1) \ll 1$. We can then use the small angle formula to simplify the cosine:

$$\begin{aligned}
\cos\big(\omega t(\cos\theta - \cos\theta')\big) &= \cos(\omega t(\cos\theta - \cos(\theta - \Delta\theta)) \\
&= \cos(\omega t(\cos\theta - \cos\theta\cos\Delta\theta - \sin\theta\sin\Delta\theta)) \\
&\cong \cos(\omega t(\cancel{\cos\theta} - \cancel{\cos\theta} - \Delta\theta\,\sin\theta)) \\
&= \cos(\omega t\,\Delta\theta\sin\theta) = \cos(\omega_d\, t\sin\theta),
\end{aligned}$$

where $\omega_d = \omega\,\Delta\theta$.

The function we need to evaluate is:

$$f_1(t) = \frac{4(d+1)}{\pi}\int_0^\pi f(\theta,\, \theta')\cos(\omega_d\, t\sin\theta)\, d\theta, \tag{2.24}$$

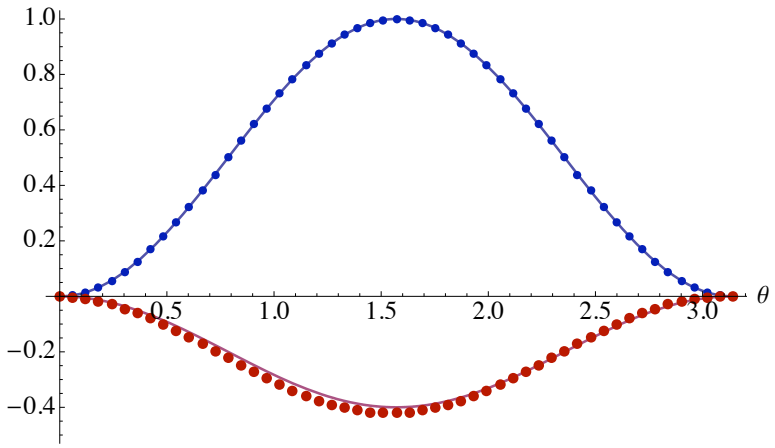

Figure 9: Comparison between $f(k,k)$ *[upper blue points]*, $f(k,k+1)$ *[lower red points]* and sine approximations for $d = 51$. The $k' = k$ points agree precisely with the sine, whereas there is a small deviation for the $k' = k \pm 1$ terms.

If we plot $f(\theta, \theta')$ just along the lines $k' = k \pm 1$ (shown in Fig. 9), we see that we can reasonably approximate it by $-2/5 \sin^2\theta$.[7] Since we assume $d \gg 1$, we can simplify the expression to:

$$f_1(t) \cong -\frac{8d}{5\,\pi} \int_0^\pi \sin^2\theta \cos(\omega_d\, t \sin\theta)\, d\theta. \tag{2.25}$$

To aid in the integration, we will add another term to f_1, but one that evaluates to zero. That is, we will integrate

$$f_1(t) = -\frac{4d}{5}\left(\frac{2}{\pi}\int_0^\pi \sin^2\theta \cos(\omega_d\, t \sin\theta) - \frac{2}{\pi}\int_0^\pi \cos\theta \sin\theta \sin(\omega_d\, t \sin\theta)\right) d\theta. \tag{2.26}$$

With a little effort, this can be manipulated into the form

$$\begin{aligned} f_1(t) &= \frac{4d}{5}\left(\frac{1}{\pi}\int_0^\pi \cos(\omega_d\, t \sin\theta - 2\theta) - \frac{1}{\pi}\int_0^\pi \cos(\omega_d\, t \sin\theta)\right)\, d\theta \\ &= \frac{4d}{5}\left(J_2(\omega_d\, t) - J_0(\omega_d\, t)\right). \end{aligned} \tag{2.27}$$

Bessel functions reappear! This approximation is only valid in the continuum limit, as d becomes large, but in that limit, we find the agreement with the

[7] This can be verified by exact treatment of the sum Eq. 2.23.

sums to be quite good. The average depth can then be expressed as

$$d_{avg}(t) = f_0 + f_1(t) = d + \frac{4d}{5}\left(J_2(\omega_d\, t) - J_0(\omega_d\, t)\right). \tag{2.28}$$

We not only see that the walk oscillates between the two ends of the graph, with gradually diminishing amplitude, but also that the period of oscillation is determined by $\omega_d = \omega\,\pi/2(d+1)$. Thus, the period scales with the length of the graph, which again agrees with the hypothesis of linear propagation. So long as the walk remains ideal, the column space analysis fully captures the walk dynamics, but the situation becomes more complicated when imperfections are introduced.

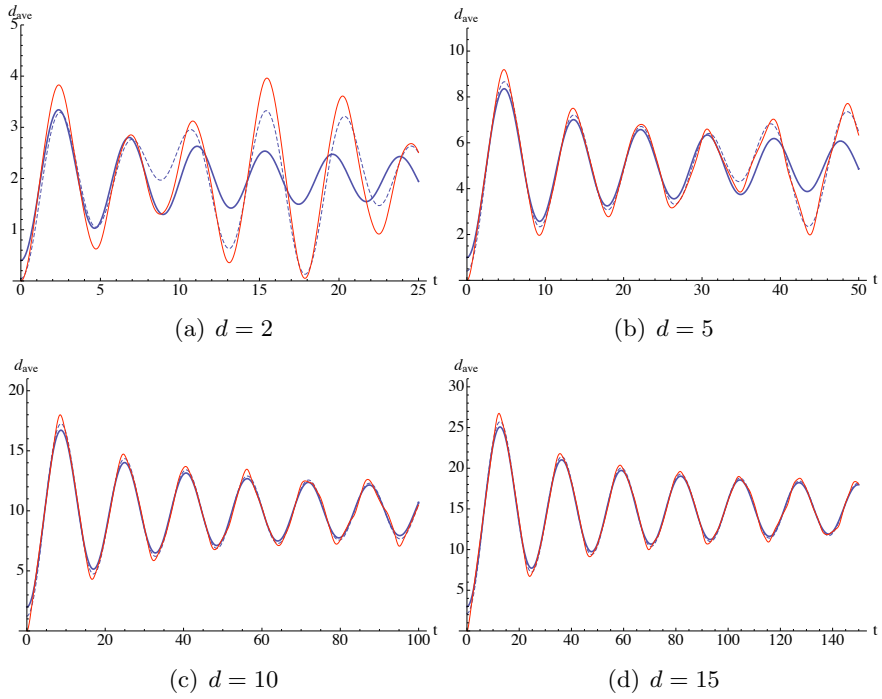

(a) $d = 2$ (b) $d = 5$

(c) $d = 10$ (d) $d = 15$

Figure 10: Comparison between the exact value *[solid light red]*, truncated sum ($k' = k$, and $k' = k \pm 1$) *[dashed light blue]* and continuum approximation *[solid heavy blue]* for the average depth d_{avg} as a function of t and various values of d. The approximations undershoot, but improve visibly as the depth d increases.

2.5 The full Glued Trees spectrum

So long as we are only concerned with the evolution in the column space, the eigenstates we found previously are all that can be accessed. However, the Hilbert space of the graph is much larger than the l-dimensional column space, and hence there are many other eigenstates of the graph. These play a significant role when considering the effects of weak disorder.

If we observe that the glued trees graph is self-similar, then a simple hierarchy becomes apparent: each glued trees graph G_d contains 2^ν subgraphs, each equivalent to $G_{d-\nu}$. Furthermore, these subgraphs can be grouped into $2^{\nu-1}$ pairs of subgraphs formed by removing the roots of a larger graph equivalent to $G_{d-\nu+1}$. This is illustrated for $d = 3$ in Fig. 11, where two copies of G_2 result from the removal of vertices 1 and 22, and similarly two copies of G_1 are produced by removing vertices 2 and 20 (or 3 and 21).

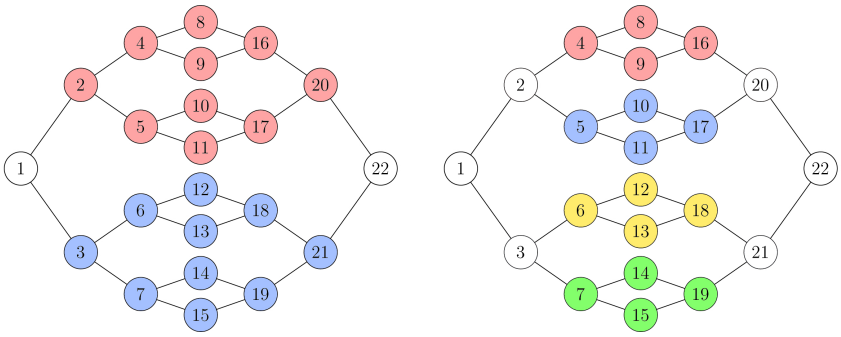

(a) The subgraphs equivalent to G_2 (b) The subgraphs equivalent to G_1

Figure 11: The subgraphs of G_3

If we consider the subspaces formed by each pair of subgraphs, we can see that an equal but opposite-signed superposition over the paired subgraphs also allows for stationary states, as the opposite phase portions interfere destructively at the two nodes that connect the subgraph pair (e.g. vertices 1 and 22 in Fig. 11(a)). To see this, let $|\,\Psi^{G_{d'}}_{k,\,d'}\,\rangle$ represent a column space eigenstate of the graph $G_{d'}$. Then if $G^1_{d-\nu}$ and $G^2_{d-\nu}$ are paired subgraphs of the graph G_d (each equivalent to $G_{d-\nu}$), the state

$$|\,\Psi_{\nu,k,d}\,\rangle = \frac{1}{\sqrt{2}}\left(|\,\Psi^{G^1_{d-\nu}}_{k,\,d-\nu}\,\rangle - |\,\Psi^{G^2_{d-\nu}}_{k,\,d-\nu}\,\rangle\right), \quad \text{for } 0 \le \nu \le d \tag{2.29}$$

is a new eigenstate of G_d, with eigenvalue $E_{k,\,d-\nu}$. Note that the states mentioned above all reside in the larger Hilbert space of G_d.

Recall that for a given ν, there are $2^{d-\nu}$ choices of G^1 and G^2. Thus, the spectrum of the GT graph is substantially degenerate, with $E = 0$ having the highest multiplicity. Specifically, there are 2^d eigenstates with energy $E = 0$ – one in the column space, and then one per pair of subgraphs, including 2^{d-1} in the central column alone (the singlet states).

Having established the structure of the spectrum, let us now make the notation more succinct. We define the following:

1. The sub-column space C_i is the column space of the paired subgraphs, which are connected on the left side of the graph by the vertex i. For example, we would denote the column space over the two subgraphs in Fig. 11(a) by C_1 and those in Fig. 11(b) by C_2 and C_3 respectively.

2. The sub-column-state $|\,\mathrm{col}_i\; j\,\rangle$ is the j^{th} column state of C_i.

3. The sub-column space eigenstate $|\,\Psi_k^i\,\rangle$ is the k^{th} eigenstate of C_i.

Similarly, we define $C_{(\nu)}$, $|\,\mathrm{col}_{(\nu)}\; j\,\rangle$ and $|\,\Psi_k^{(\nu)}\,\rangle$ to be the set of C_i, $|\,\mathrm{col}_i\; j\,\rangle$ and $|\,\Psi_k^i\,\rangle$ respectively, where $i \in \mathrm{col}\ (\nu - 1)$. That is, the first vertex state in each of the three is in col ν. Using this convention, the full column space is $C_{(0)}$, while the pair of subgraphs in Fig. 11(a) correspond to $C_{(1)}$, and the four in Fig. 11(b) correspond to $C_{(2)}$. The notation will be of most use in our discussion of Fermi's Golden Rule, in the following chapter.

2.6 Discussion

In this chapter, we have derived a number of results concerning the Glued Trees graph. In particular, we have determined the spectral structure of the graph, and used this to understand how an initially localized wavefunction propagates in time. We find that the amplitude at any site is given by an infinite series of Bessel functions, and this dependence results in a linearly propagating wavefunction, moving at a velocity $\omega = 2\sqrt{2}\,\gamma$. Defining the average depth, d_{avg}, we note that this quantity is oscillatory, with an amplitude that decays slowly. Such behavior can be interpreted as a wavepacket that sloshes back and forth between the ends of the graph, being reflected upon hitting the roots. Another expectation we might have is that the wavepacket will tend to spread out in time, obeying the dispersion relation determined by the energy spectrum. Evidence for this is found in the numerical results to be presented in Chapter 4.

To gain a better understanding of the differences between the classical and quantum cases, we can apply a similar analysis to the classical walk.

In this case, we are not allowed to make the simplifications of disregarding the degree of the graph vertices, and hence we use the graph's Laplacian to define the infinitesimal generator matrix for the continuous time random walk (see Section 1.1). However, we can still reduce the system to a line representation. Numerical solutions give us the eigenvalues and eigenvectors on the line, so we can easily find the time evolved probability distribution given by Eq. 1.7. Figure 12(a) shows the evolution of the probability on the graph, which shows the diffusive behavior of the classical walk clearly – the probability quickly transfers to the center of the graph, where it then becomes exponentially localized.

The subsequent plot shows the average depth reached by the classical walker. Unlike the oscillatory wavepacket motion of the quantum walk, the classical walk resembles an exponential decay towards the center of the graph, and d_{avg} never rises past d. This distinction is responsible for the celebrated exponential speedup enjoyed by the quantum walk.

We can also derive the exponential speedup mathematically. Recall that the approximate Green's function for the quantum walk is (Eq. 2.17)

$$G(0,\, j,\, t) \quad = \quad i^j \frac{2j}{\omega t} J_{j+1}(\omega t).$$

The peak of this function can only be determined numerically, but for larger values of j, it is close to $\tau_j = j/\omega = j/2\sqrt{2}\gamma$, which agrees with the prediction of linear propagation at the velocity $2\sqrt{2}\gamma$. The height of the peak is likewise a numerically calculated result, but comes out close to $1/\sqrt{l}$ at the end node – substantially larger than the classical hitting probability. The conclusion is that the quantum walker crosses the graph in an exponentially shorter time than the classical walker.

Now that we know the expected behavior of the ideal quantum walk on the GT graphs, we will proceed to explore the effects of noise, in the form of static disorder, on the wavefunction propagation. A reasonable hypothesis is that the disruption will reduce the rate of transport, causing something resembling a transition from quantum ballistic propagation to classical diffusive propagation. In the following chapter, we will derive several models to describe the effects of disorder, culminating in a dynamical model for calculating the walk's evolution in the presence of disorder.

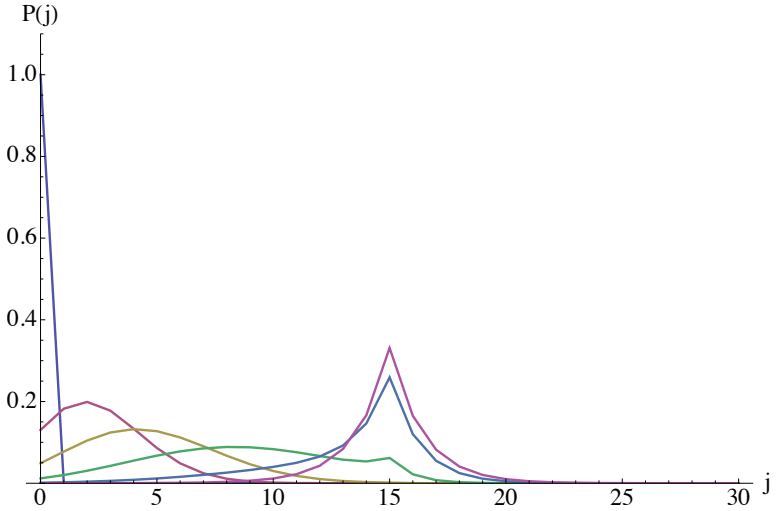

(a) The probability distribution $P(j)$ on the column space plotted at times $t = 0$, 2, 4, 8, 16, 32.

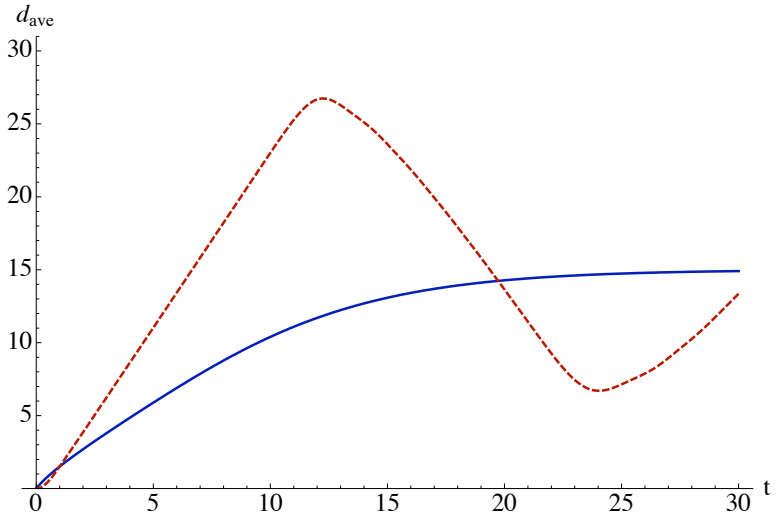

(b) The classical average depth, d_{avg} *[solid blue curve]*, compared with the quantum result, *[dashed red curve]*

Figure 12: The propagation of the classical walker on G_{15}

3 Disorder, Localization and Decay

3.1 Motivations

> *Quantum phenomena do not occur in a Hilbert space; they occur in a laboratory.*
>
> Asher Peres

Jokes about spherical cows *in vacuo* notwithstanding, we as physicists are ultimately concerned with physical reality, and not the idealized behavior of theoretical constructs. An understanding of any sort of phenomena, therefore, necessarily involves their implementation in actual physical systems. It is a fact that exact precision and isolation are impossible to come by in our messy, warm and noisy environment. Consequently, we cannot construct machines that perfectly simulate most systems, particularly as we enter the quantum mechanical regime. It is necessary, then, to understand the effects of noise on the systems that we would like to simulate.

All of the above applies to quantum walks, and certainly to quantum walks on the Glued Trees. The effects of noise on the GT and similar graphs have in fact already been the subject of much study [KLMW07, Ken07]. In this chapter, we will apply perturbation theory to the disordered GT walks, ultimately deriving a local decay model that describes the end-to-end propagation of the GT walk.

3.2 Fundamental concepts

Disorder-induced localization

In his 1958 study of electron transport in disordered lattices, Anderson presented the result that static site disorder (in the form of variations in energy between atoms) led to localization; quantum interference effects inhibit state transfer over substantial distances [And58]. The degree of localization depends on the dimensionality of the system.[8] In particular, it has been shown that in 1D, the uniqueness of paths connecting separate states mandates that the eigenstates of the system be exponentially localized [Bor63, EC71]. This condition is relaxed in higher dimensions, where obstructions might be avoided, so to speak. The 2D case is the critical dimension, above which there are states that are not exponentially localized, although disorder does in general inhibit quantum transport [AALR79].

[8] In the sense of spatial dimensions, rather than the dimension of the Hilbert space.

The topic of disordered walks on the Glued Trees has been investigated previously by Keating et al. [KLMW07]. By simulating walks on the column space in the presence of diagonal disorder of the form in Eq. 1.15

$$\mathcal{H}_{\text{col}}{}' = \mathcal{H}_{\text{col}} + \sum_{j=0}^{2d} \epsilon_j |\, \tilde{\text{col}}\, j \,\rangle\langle\, \tilde{\text{col}}\, j \,|,$$

they found that the wavefunction of the walker demonstrated clear signs of localization, with the probability distribution dropping off exponentially with the distance from the starting point. Such a situation would be catastrophic for any attempt at quantum walk-based computations. However, the situation may not be quite so dire.

Since exponential localization is inevitable on one-dimensional systems, regardless of the strength of disorder, the result found by Keating et al. was in some sense a foregone conclusion, since their simulations took place in a one-dimensional lattice. Hence, extrapolating from their result to predict localization on the full graph may not give the full picture. It turns out that the analytical calculations for Anderson localization can be carried out exactly on the Bethe lattice or 'Cayley Tree', essentially an infinite tree with fixed degree. In the case with connectivity $K = 2$, this is simply an infinite binary tree. Several studies predict a localization transition at a critical strength of disorder, beyond which the conductance vanishes [ACTA73, JG79, GJ80]. Below this critical value, there exist extended states on the graph, allowing for varying degrees of transport. These results are of particular interest, since before a walker reaches the center of the graph, it essentially sees no difference between a Cayley tree and a GT graph. Hence, we expect that if the Cayley tree possesses extended states for small disorder, so should the GT graph, in contradiction of Keating's findings. Our results (presented in the next chapter) bear out this conjecture.

Rather than simulate diagonal disorder in the context of the column space Hamiltonian, as in Keating's model, we choose to implement the evolution on the full graph, starting with site disorder, and comparing the results with the effects of bond disorder. While extending the calculations to graphs of the size considered by Keating ($d \sim 500$) is computationally unfeasible, we have covered a range of smaller graphs ($d \in [5, 23]$, with $N_d \in [94, 25 \times 10^7]$). Besides the simulations, we have also derived three models for the effects of disorder, which will be developed in this section.

Apart from the dimensionality of the problem, one other objection to Keating's findings can be raised. Specifically, it is unclear what the diagonal disorder in the column space might correspond to physically. On-site

energies that vary independently from site to site are intuitively the sort of disruptions we might expect from imperfect experimental control, but variations that are correlated over collections of many sites (i.e. GT columns) are less well motivated. Studies on the hypercube have shown the two paradigms to be vastly different. Specifically, when studied using Strauch's (arguably more egalitarian) 'vertex model' [Str09], the hypercube shows a substantial robustness against disorder, with a small but finite asymptotic value for the hitting probability, given some fixed disorder/decoherence strength as the graph size increases, whereas the hitting probability vanishes for large graphs in the 'subspace model' of Alagíc and Russell [AR05]. The former case essentially Golden Rules out localization, likely due to the hypercube's high dimensionality. Similar results might be expected for the GT, since it is intermediate in structure between the line and the hypercube.

Quantum decay

Decay being a recurring theme in Nature, it is unsurprising that the investigation of unstable states has a long history. A notable pioneer in the field was Gamow, who provided a derivation of alpha decay [Gam28]. A standard paradigm in quantum decay is the presence of a single state coupled to a continuum. As an example, we might consider an excited state of a hydrogen atom, which may decay, releasing a photon in an arbitrary direction. For such states, it is generally held that the probability of being in the preferred state diminishes exponentially in time, but with important deviations at short and very long times.

Noting that criteria on 'physical feasibility' contradict the results of exponential decay, Khalfin pointed out that at short times, we cannot neglect the existence of a non-exponential term, which leads to initial decay that is slower than exponential [Kha58]. This slower decay allows frequent measurements to retard decay (known as the quantum Zeno effect or 'watched pot' effect), although Schulman, Ranfagni and Mugnai have demonstrated that other measurements can also accelerate decay (a.k.a. the anti-Zeno effect) [SRM94].

After this short-time evolution, the exponential law holds basically for timescales on which there is substantial probability in the unstable state. At long times, as the probability in the final states build up, reverse flow can regenerate the original state, once more producing slower-than-exponential decay [FGR78]. Another relevant phenomenon is that of limited quantum decay, in which eigenstates fail to decay due to their energies being outside the range of final state energies [GS95].

Fermi's Golden Rule

A standard tool in the study of quantum decay is the 'Golden Rule', so named by Fermi for its widespread applicability. The Golden Rule Golden Rule states that, when we have a single initial state that is coupled by a small perturbation V to a continuum of states, we expect the decay from the initial state $|\,\psi_0\,\rangle$ to one of the continuum states $|\,\phi_\alpha\,\rangle$ to be governed by a decay rate of the following form [Sch68]:

$$\Gamma_\alpha = \frac{2\pi}{\hbar}|\langle\,\phi_\alpha\,|V|\,\psi_0\,\rangle|^2\rho(\alpha) \tag{3.1}$$

where α is a continuously varying parameter, and $\rho(\alpha)$ is the density of states at the corresponding energy,

$$\rho(\alpha) = \left.\frac{\Delta N}{\Delta E}\right|_\alpha . \tag{3.2}$$

In other words, the decay rate is proportional to the absolute value squared of the matrix element of the perturbation that couples the initial and final states and the density of states. Such decays typically conserve the energy of the system, which is to say that the initial state only decays directly to states that are close in energy.

As the Golden Rule depends on the decay being one-directional, in the sense that the decay products do not return to the initial state, it is inapplicable at long times, when there has been a substantial buildup of probability in the final states. If the initial state is not an eigenstate of the unperturbed Hamiltonian, the decay may involve multiple decay rates, and hence will show a more complicated profile than a straightforward exponential decrease. Finally, while the Golden Rule can be applied to discrete systems, it is only truly effective in the continuum limit, i.e. when the number of final states is large, and the energy spacing of the spectrum relatively small.

3.3 Decay from the column space

The fast traversal of the Glued Trees graph by a quantum walker is a result of the graph's extensive symmetry, and hence if the symmetry of the wavefunction on the graph is lost, the interference effects that lead to rapid traversal are lost. In particular, if we introduce disorder to the Hamiltonian, the components of the wavefunction following different paths on the graph will accumulate random phases that will interfere destructively. An immediate consequence is that the walk will depart from the column space, inhibiting propagation.

To study the decay from the column space, a quantity of obvious interest is the column space probability, p_{col}, defined for some wavefunction $|\,\psi(t)\,\rangle$ as:

$$p_{col}(t) = \sum_{j=0}^{2d} |\langle\, \text{col } j \,|\, \psi(t)\,\rangle|^2 \,. \tag{3.3}$$

The column states $|\,\text{col } j\,\rangle$ are defined as in Eq. 2.3. This quantity not only provides a convenient measure of propagation, but also serves as a (very) rough upper bound on the hitting probability. [9]

Since the disordered Hamiltonian remains nevertheless a unitary operator, we do expect to observe quantum recurrences, in which the system comes arbitrarily close to its initial state. However, the time scales involved for such a recurrence are far longer than the time required for a walker to cross the graph. So, we can essentially assume – at least for weak disorder – that the portion of the wavefunction that has decayed from the column space does not return.

With that assumption, we now present three models of the column space decay under diagonally disordered Hamiltonians. Comparisons with the numerical results will be shown in the following chapter.

[9] In most of this chapter, we will work in the full Hilbert space rather than the line representation, hence column space states and eigenstates will generally be notated without tildes. The only exceptions are when we are discussing the various column-space models.

3.4 Models of decay

Short-time decay

Our first approximation is a short time calculation of the column space probability, found by taking the first order Taylor expansion of the Hamiltonian. We will keep terms of up to $\mathcal{O}(t^2)$. Given some initial starting state, $|\,\psi_0\,\rangle$, the column space probability at time t is given by

$$\begin{aligned}
p_{col}(t) &= \sum_{j=0}^{2d} |\langle\,\text{col } j\,|\,\psi(t)\,\rangle|^2 \\
&= \sum_{j=0}^{2d} \left|\langle\,\text{col } j\,|e^{-i\,\mathcal{H}\,t}|\,\psi_0\,\rangle\right|^2 \\
&= \sum_{j=0}^{2d} \langle\,\text{col } j\,|e^{-i\,\mathcal{H}\,t}|\,\psi_0\,\rangle\,\langle\,\psi_0\,|e^{i\,\mathcal{H}\,t}|\,\text{col } j\,\rangle \\
&\cong \sum_{j=0}^{2d} \langle\,\text{col } j\,|(1 - i\,\mathcal{H}\,t - \frac{t^2}{2}\,\mathcal{H}^2)|\,\psi_0\,\rangle\,\langle\,\psi_0\,|(1 + i\,\mathcal{H}\,t - \frac{t^2}{2}\,\mathcal{H}^2)|\,\text{col } j\,\rangle.
\end{aligned} \tag{3.4}$$

Expanding out the terms of the summand gives the following expression:

$$\begin{aligned}
p_{col}(t) = \sum_{j=0}^{2d} & |\langle\,\text{col } j\,|\,\psi_0\,\rangle|^2 + t^2|\langle\,\text{col } j\,|\,\mathcal{H}\,|\,\psi_0\,\rangle|^2 \\
& + it\,(\langle\,\text{col } j\,|\,\mathcal{H}\,|\,\psi_0\,\rangle\langle\,\psi_0\,|\,\text{col } j\,\rangle - \langle\,\psi_0\,|\,\mathcal{H}\,|\,\text{col } j\,\rangle\langle\,\text{col } j\,|\,\psi_0\,\rangle) \\
& - \frac{t^2}{2}\left(\langle\,\text{col } j\,|\,\psi_0\,\rangle\langle\,\psi_0\,|\,\mathcal{H}^2\,|\,\text{col } j\,\rangle + \langle\,\psi_0\,|\,\text{col } j\,\rangle\langle\,\text{col } j\,|\,\mathcal{H}^2\,|\,\psi_0\,\rangle\right).
\end{aligned} \tag{3.5}$$

Note that the contents of both parentheses in Eq. 3.5 are complex conjugates. As a result of this, and the fact that the Hamiltonian and column states are both real, the choice of a real starting state ψ_0 (or one with an arbitrary overall phase) allows us to simplify the equation further – the linear term vanishes, to give:

$$\begin{aligned}
p_{col}(t) \;=\; & \sum_{j=0}^{2d} |\langle\,\text{col } j\,|\,\psi_0\,\rangle|^2 + t^2|\langle\,\text{col } j\,|\,\mathcal{H}\,|\,\psi_0\,\rangle|^2 \\
& -\; t^2\left(\langle\,\text{col } j\,|\,\psi_0\,\rangle\langle\,\psi_0\,|\,\mathcal{H}^2\,|\,\text{col } j\,\rangle\right).
\end{aligned} \tag{3.6}$$

We now consider starting states taken from the column states of the graph, i.e. $|\,\psi_0\,\rangle = |\,\mathrm{col}\;j_0\,\rangle$. Then, the orthonormality of the column states leaves only one sum,

$$p_{col}(t) \;=\; 1 - t^2 \left(\langle\,\mathrm{col}\;j_0\,|\,\mathcal{H}^2\,|\,\mathrm{col}\;j_0\,\rangle - \sum_{j=0}^{2d} |\langle\,\mathrm{col}\;j\,|\,\mathcal{H}\,|\,\mathrm{col}\;j_0\,\rangle|^2 \right). \quad (3.7)$$

Let us write out in full the squared matrix element sum,

$$\begin{aligned} \sum_{j=0}^{2d} |\langle\,\mathrm{col}\;j\,|\,\mathcal{H}\,|\,\mathrm{col}\;j_0\,\rangle|^2 \;&=\; \sum_{j=0}^{2d} \langle\,\mathrm{col}\;j_0\,|\,\mathcal{H}\,|\,\mathrm{col}\;j\,\rangle\langle\,\mathrm{col}\;j\,|\,\mathcal{H}\,|\,\mathrm{col}\;j_0\,\rangle \\ &=\; \langle\,\mathrm{col}\;j_0\,|\,\mathcal{H}\left(\sum_{j=0}^{2d} |\,\mathrm{col}\;j\,\rangle\langle\,\mathrm{col}\;j\,|\right)\mathcal{H}\,|\,\mathrm{col}\;j_0\,\rangle \\ &=\; \langle\,\mathrm{col}\;j_0\,|\,\mathcal{H}\,P\,\mathcal{H}\,|\,\mathrm{col}\;j_0\,\rangle, \end{aligned} \quad (3.8)$$

where operator P is simply the column space projector (Eq. 2.7), which commutes with the ideal Hamiltonian.

Consider first the case $\mathcal{H} = \mathcal{H}_0$. Since $\mathcal{H}_0\,|\,\mathrm{col}\;j_0\,\rangle$ is in the column space, and P acting on a column space state merely leaves the state untouched, Eq. 3.8 simplifies to

$$\langle\,\mathrm{col}\;j_0\,|{\mathcal{H}_0}^2|\,\mathrm{col}\;j_0\,\rangle \;=\; \sum_{j=0}^{2d} |\langle\,\mathrm{col}\;j\,|\,\mathcal{H}_0\,|\,\mathrm{col}\;j_0\,\rangle|^2,$$

or equivalently,

$$\langle\,\mathrm{col}\;j_0\,|{\mathcal{H}_0}^2|\,\mathrm{col}\;j_0\,\rangle \;-\; \sum_{j=0}^{2d} |\langle\,\mathrm{col}\;j\,|\,\mathcal{H}_0\,|\,\mathrm{col}\;j_0\,\rangle|^2 \;=\; 0;$$

the ideal Hamiltonian does not contribute to the quadratic term in Eq. 3.7.

To find the column space probability in the presence of diagonal disorder, $\mathcal{H} = \mathcal{H}_0 + \mathcal{H}_s$, we let

$$\mathcal{H}_s = \sum_{i=1}^{N_d} \epsilon_i |\,i\,\rangle\langle\,i\,|.$$

As the perturbation $\mathcal{H}_s$ is diagonal in the vertex basis, it does not couple distinct column spaces to each other, and so

$$\langle\,\mathrm{col}\;j\,|\,\mathcal{H}_s\,|\,\mathrm{col}\;j_0\,\rangle = 0, \quad (3.9)$$

for $j \neq j_0$. Terms involving $\mathcal{H}_s \mathcal{H}_0$ likewise disappear. Consequently, we need only use the perturbation $\mathcal{H}_s$ in Eq. 3.7. So, we calculate the column space probability to be:

$$\begin{aligned} p_{col}(t) &= 1 - t^2 \left(\langle \text{ col } j_0 \,|{\mathcal{H}_s}^2|\, \text{col } j_0 \rangle - \sum_{j=0}^{2d} |\langle \text{ col } j \,|\, \mathcal{H}_s \,|\, \text{col } j_0 \rangle|^2 \right) \\ &= 1 - t^2 \left(\langle \text{ col } j_0 \,|{\mathcal{H}_s}^2|\, \text{col } j_0 \rangle - |\langle \text{ col } j_0 \,|\, \mathcal{H}_s \,|\, \text{col } j_0 \rangle|^2 \right) \\ &= 1 - t^2 / {N_{j_0}}^2 \sum_{i,j \in \text{col } j_0} \epsilon_i \, \epsilon_j \, (N_{j_0} \delta_{i,j} - 1), \end{aligned} \tag{3.10}$$

We can separate the sums of the squared terms and cross-terms, where we are still summing over the vertex labels in col j_0.

$$p_{col}(t) = 1 - t^2 / {N_{j_0}}^2 \left((N_{j_0} - 1) \sum_i {\epsilon_i}^2 - \sum_{i \neq j} \epsilon_i \, \epsilon_j \right). \tag{3.11}$$

Up till now, we have said nothing about the distribution of the disorder terms on the graph. We will presently assume that they are randomly distributed, following a probability distribution that is symmetric about 0, and with a finite variance σ^2. In practice, our simulations implement disorder with a uniform distribution on some range $|\epsilon_i| \leq \varepsilon$, in which case we have $\sigma^2 = \varepsilon^2/3$. These assumptions allow us to find the expectation value of the column space probability[10],

$$\langle p_{col}(t) \rangle = 1 - t^2 / {N_{j_0}}^2 \left((N_{j_0} - 1) \sum_i \langle {\epsilon_i}^2 \rangle - \sum_{i \neq j} \langle \epsilon_i \, \epsilon_j \rangle \right). \tag{3.12}$$

Since the disorder terms have a mean of zero, the expectation values of the cross-terms vanish, $\langle \epsilon_i \, \epsilon_j \rangle = \langle \epsilon_i \rangle \langle \epsilon_j \rangle = 0$, while the expected value of the squared terms is simply the variance, $\langle {\epsilon_i}^2 \rangle = \sigma^2$. This gives us a surprisingly simple result,

$$\langle p_{col}(t) \rangle = 1 - t^2 \sigma^2 \, \frac{N_{j_0} - 1}{N_{j_0}} = 1 - t^2 \sigma^2 \left(1 - \frac{1}{N_{j_0}} \right). \tag{3.13}$$

[10] It turns out that the sum in parentheses is also equivalent to the squares of the pairwise differences between the on-site energies $(\epsilon_i - \epsilon_j)^2$. This makes a good deal of sense, as it is the unevenness of the energies that gives to the interference between vertex states in the same column.

That is to say, we expect the column space probability to decay quadratically at a rate that increases with the number of vertices in the initial column state. If we somewhat naïvely extrapolate this result to the exponential decay regime, we might expect the rate of decay Γ_{j_0} starting in a column-space state to scale as

$$\Gamma_{j_0} \;\propto\; \sigma^2(1 - 1/N_{j_0}) \;\leq\; \sigma^2(1 - 2^{-d}). \tag{3.14}$$

Observe that the RHS quickly approaches σ^2 as we move towards the center of large graphs. This agrees with our intuitions, and with some aspects of the decay that we observe in simulations. The reason we might expect the decay to accelerate closer to the center of the graph is that, with more vertices in each column, there is more room for phase differences that will push the state out of the column space, and furthermore each column state overlaps (and hence couples to) more the eigenstates of the graph's full spectrum.

A comparison with simulation demonstrates that although the character of the short-time decay is correct, it is valid only for relatively short times. This calculation also gives no clues about the final states to which the probability is leaking, and is dimensionally incorrect (it has units of energy squared, rather than of inverse time). For additional insights on the decay, and a clearer understanding of the mechanisms behind it, we invoke Fermi's Golden Rule.

Fermi's Golden Rule applied

In Chapter 2, we described the spectrum of the Glued Trees graph in detail, in particular the large number of degenerate eigenstates. In the limit of large graphs, we might reasonably apply Fermi's Golden Rule to describe the decay from the column space, as much of the decay will take place well before the wavepacket reaches the center of the graph. Then, the probability decays primarily into the outermost sub-column spaces, which are most closely described by the continuum limit. We will begin by considering the decays from the column space eigenstates, computing the matrix elements for the decay.

Recall that the Golden Rule Golden Rule states that the decay rate Γ obeys Eq. 3.1,

$$\Gamma_\alpha = \frac{2\pi}{\hbar} |\langle \phi_\alpha | V | \psi_0 \rangle|^2 \rho(\alpha).$$

In the context of the decay from the column space, we let $|\psi_0\rangle$ be one of the column space eigenstates $|\Psi_k\rangle$, and $|\phi_\alpha\rangle$ be drawn from the sub-column space eigenstates $|\Psi^i_{k'}\rangle$. So, we can let α be represented instead

by the discrete indices i and k'. The perturbation V is simply the diagonal matrix of on-site energies ϵ_i. Finally, we can disregard the factor of $\hbar$ – in fact, we have been working the entire time in units where $\hbar = 1$.

To set up the matrix element calculation, we first express the eigenstates $|\,\Psi_k\,\rangle$ and $|\,\Psi^i_k\,\rangle$ in terms of (sub)column space representations. We can assume without loss of generality that $i = 2^\nu$, for some integer $\nu \leq d$, i.e. the sub-column space C_i is the 'top' one in $C_{(\nu)}$ – the matrix element with all the sub-column spaces at a given depth ν are identical.

$$|\,\Psi_k\,\rangle = \frac{1}{\sqrt{d+1}} \sum_{j=0}^{2d} \sin\!\left(\frac{k\,(j+1)\,\pi}{2(d+1)}\right) |\,\mathrm{col}\; j\,\rangle$$

$$|\,\Psi^i_{k'}\,\rangle = \frac{1}{\sqrt{d-\nu+1}} \sum_{j'=0}^{2(d-\nu)} \sin\!\left(\frac{k\,(j'+1)\,\pi}{2(d-\nu+1)}\right) |\,\mathrm{col}_i\; j'\,\rangle.$$

The matrix element can be written explicitly as

$$\begin{aligned} M_{k,\,k',\,\nu} &= \langle\,\Psi^i_{k'}\,|\,V\,|\,\Psi_k\,\rangle \\ &= \left(\sum_{j'=0}^{2(d-\nu)} \frac{\sin\!\left(\frac{(j'+1)k'\pi}{2(d-\nu+1)}\right)}{\sqrt{(d-\nu)+1}} \langle\,\mathrm{col}_i\; j'\,|\right) V \left(\sum_{j=0}^{2d} \frac{\sin\!\left(\frac{(j+1)k\pi}{2(d+1)}\right)}{\sqrt{d+1}} |\,\mathrm{col}\; j\,\rangle\right). \end{aligned} \tag{3.15}$$

Because the perturbation is diagonal, the contributions to the matrix element only come from the combinations where the column states line up, i.e. when $\mathrm{col}_i\, j' \subset \mathrm{col}\, j$. So our sum over the column states will be reduced to those in the range $\nu \leq j \leq 2d - \nu$. Hence,

$$M_{k,\,k',\,\nu} = \left(\sum_{j'=0}^{2(d-\nu)} \frac{\sin\!\left(\frac{(j'+1)k'\pi}{2(d-\nu+1)}\right)}{\sqrt{(d-\nu)+1}} \langle\,\mathrm{col}_i\; j'\,|\right) V \left(\sum_{j=\nu}^{2d-\nu} \frac{\sin\!\left(\frac{(j+1)k\pi}{2(d+1)}\right)}{\sqrt{d+1}} |\,\mathrm{col}\; j\,\rangle\right). \tag{3.16}$$

If we now go ahead and take the absolute value squared of the matrix element, we will end up with an expression that includes the square of a sum over disorder terms. We then take the expectation value of the matrix element. By similar arguments to those in the derivation of the short time decay, only the squared terms should remain, and these will be replaced by the variance of the disorder terms.

Let us consider the action of the perturbation on a single column state $|\,\mathrm{col}\;j\,\rangle$. The vertex states that comprise the column state will each pick up their corresponding disorder term:

$$V|\,\mathrm{col}\;j\,\rangle = \frac{1}{\sqrt{N_j}} \sum_{\mu\,\in\,\mathrm{col}\,j} \epsilon_\mu\,|\,\mu\,\rangle.$$

Without loss of generality, we can assume that $j \leq d$, i.e. $|\,\mathrm{col}\;j\,\rangle$ is not on the right side of the graph. Then it contains $N_j = 2^j$ vertices, each weighted by $1/\sqrt{N_j}$. We then take the inner product of this column state with the sub-column-state $|\,\mathrm{col}_i\;(j-\nu)\,\rangle$, where we have set $j' = j - \nu$ to match up indices correctly.

$$\langle\,\mathrm{col}_i\;(j-\nu)\,|\,V\,|\,\mathrm{col}\;j\,\rangle = \left(\frac{1}{\sqrt{N_{j-\nu}}} \sum_{\mu'\,\in\,\mathrm{col}_i\,j} \langle\,\mu'\,|\right)\left(\frac{1}{\sqrt{N_j}} \sum_{\mu\,\in\,\mathrm{col}\,j} \epsilon_\mu\,|\,\mu\,\rangle\right).$$

Since only the vertex states that can be paired up between $|\,\mathrm{col}\;j\,\rangle$ and $|\,\mathrm{col}_i\;(j-\nu)\,\rangle$ contribute to the inner product, we will get a sum of $N_{(j-\nu)}$ disorder terms, each divided by the factor $\sqrt{N_j\,N_{(j-\nu)}}$.

Upon squaring and taking the expectation value, the cross-terms vanish, leaving just the squared terms. Each of these has magnitude $\sigma^2/N_j\,N_{(j-\nu)}$, and there are $N_{(j-\nu)}$ such terms from each column state, so each column state contributes σ^2/N_j, modified by a sine factor. By the symmetry of the graph, we can combine the terms with $j < d$ and $j > d$, leaving us with the expectation value

$$\begin{aligned}\left\langle |M_{k,\,k',\,\nu}|^2 \right\rangle \;=\; & \frac{\sigma^2}{(d+1)(d-\nu+1)}\left[2^{-d}\sin^2\left(\frac{k\,\pi}{2}\right)\sin^2\left(\frac{k'\pi}{2}\right)\right. \\ & \left. +\;\sum_{j=\nu}^{d-1} 2^{1-j}\sin^2\left(\frac{k\,\pi(j+1)}{2(d+1)}\right)\sin^2\left(\frac{k'\pi(j-\nu+1)}{2(d-\nu+1)}\right)\right].\end{aligned} \tag{3.17}$$

We now have an expression for the quantity $M'_{k,\,k',\,\nu} = \left\langle |M_{k,\,k',\,\nu}|^2 \right\rangle$ between any column space eigenstate and any of the eigenstates of the Hamiltonian. Although we can compute this matrix element numerically with little trouble, the expression cannot be simplified in any elegant fashion. However, it is interesting to plot the magnitude of $M'_{k,\,k',\,\nu}$ for the various possibilities of k, k' and ν given some choice of d.

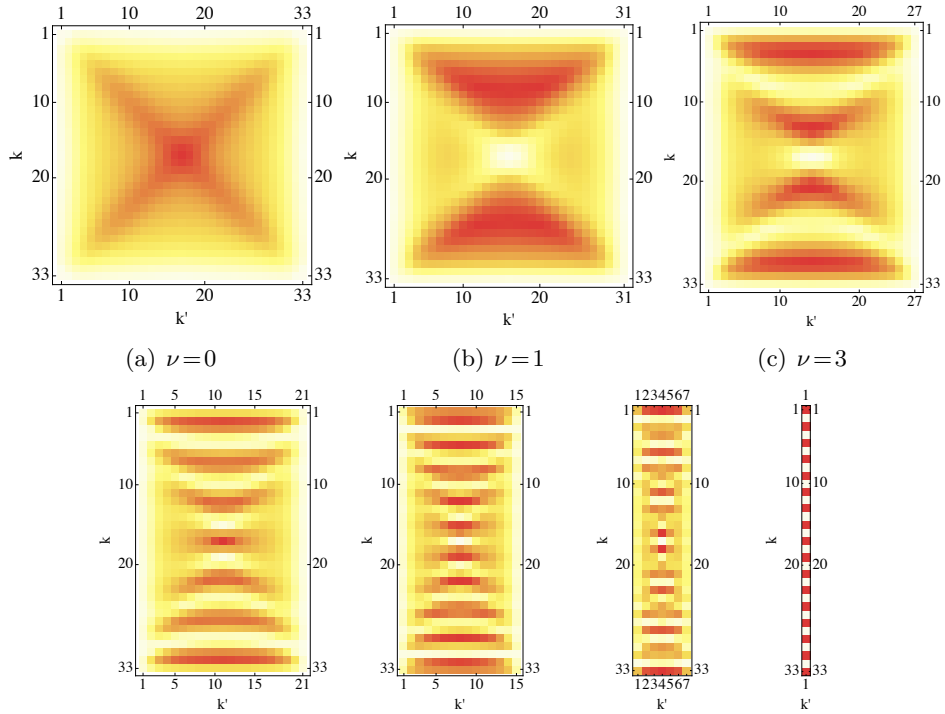

(a) $\nu=0$ (b) $\nu=1$ (c) $\nu=3$

(d) $\nu=6$ (e) $\nu=9$ (f) $\nu=13$ (g) $\nu=16$

Figure 13: Plots of the matrix element $M'_{k,k',\nu}$ for the graph G_{16}.

We can observe several interesting characteristics. First of all, we see that the decay rate into each sub-column space $C_{(\nu)}$ has a banded structure with respect to k', with the number of bands equalling $\nu + 1$. The bands emerge due to the relative overlap between the column space and non-column space eigenstates, and the increasing significance of the bands is due to the fact that, as ν grows, the number of column states overlapping the non-column space eigenstate shrinks, so the variation in the coefficient of $|\,\mathrm{col}\ j\,\rangle$ close to the center of the graph dominates the matrix element.

Of especial interest is the behavior of the $E = 0$ column space eigenstate, i.e. that with $k = d + 1$. This eigenstate has magnitude $\sin[(j + 1)\pi/2]/\sqrt{2d+1}$ at column j, that is it has magnitude 0 on the d columns with j odd, and magnitude $1/\sqrt{d+1}$ on the remaining columns. This attribute is shared by all the $E = 0$ non-column space eigenvalues, except for a shifting of the column label j. As a result, the matrix element for the energy-conserving decay displays a dramatic even-oddness, oscillating between 0 for odd ν and approximately $(8/3)2^{-\nu}$ for even ν. The $E = 0$ column space eigenstate is in fact the largest component of the starting state localized at either root, so this decay is potentially the most significant, although one should also note that the couplings from the $E = 0$ column space eigenstate to the other eigenstates in the column space are substantial, and so the decay will be somewhat complicated.

Having found the expected matrix element for a given pair of initial and final states, we now wish to find the decay rate for a choice of initial states, which involves a sum of the decay rates over all possible final states. That is, letting Γ_k represent the decay rate for the column space probability from a single eigenstate $|\,\tilde{\psi}_k\,\rangle$, we have

$$\Gamma_k = 2\pi \sum_{i=1}^{2^d-1} \sum_{k'=1}^{2(d-\nu)+1} |\langle\, \phi_{i,\,k'}\,|V|\,\tilde{\psi}_k\,\rangle|^2 \rho(i,\,k'), \tag{3.18}$$

with i indexing the chosen sub-column space, and k' the index of the eigenvalue. Here we can make one important simplification: since the matrix element is the same for all eigenvalues of a given sub-column space $C_{(\nu)}$, we can group the corresponding terms of the sum together, adding in a factor $2^{\nu-1}$ to account for the multiplicity, and then sum over ν, rather than i. Hence, we can apply the result found above for the expectation value of the matrix element, putting the decay rate in the form

$$\Gamma_k = 2\pi \sum_{\nu=1}^{d} \sum_{k'=1}^{2(d-\nu)+1} 2^{\nu-1}\, M'_{k,\,k',\,\nu}\, \rho(\nu,\,k') \tag{3.19}$$

To find the decay rate for one of the column space eigenstates using the Golden Rule Golden Rule, we will also need the density of states $\rho(E)$, but it is not immediately obvious how to calculate ρ exactly. We can proceed by estimating a constant value of ρ, separating the matrix element sum from that over the density of states. In doing so, we will take the average value of ρ,

$$\overline{\rho} \quad = \quad \frac{\sum_{\nu,k'}[\rho(\nu,\, k')]}{\sum_{\nu,k'}[1]}. \tag{3.20}$$

Let S denote the sum over the matrix elements. Then, the decay rate is given by an expression of the form:

$$\Gamma_k \;\approx\; 2\pi\, S_k\, \overline{\rho} \;=\; 2\pi \left[\sum_{\nu,k'} 2^{\nu-1} M'_{k,\,k',\,\nu}\right] \frac{\sum_{\nu,k'}[\rho(\nu,\, k')]}{\sum_{\nu,k'}[1]}. \tag{3.21}$$

Let us first calculate the average density of states. Note that for each sub-column space $C_{(\nu)}$, the following are true:

$$\begin{aligned} E_k \qquad &= \qquad 2\sqrt{2}\gamma \cos\left(\frac{k\,\pi}{2(d-\nu)+2}\right); \\ \frac{dE}{dk} \qquad &= \qquad \frac{\pi}{2(d-\nu)+2} \cdot \left[-2\sqrt{2}\gamma \sin\left(\frac{k\,\pi}{2(d-\nu)+2}\right)\right] \\ &= \qquad \frac{-2\sqrt{2}\,\pi\,\gamma}{2(d-\nu)+2}\sqrt{1-\frac{E^2}{8\,\lambda^2}}. \end{aligned} \tag{3.22}$$

It makes sense to evaluate ρ at the center of the band, where the bulk of the probability is located.

$$\begin{aligned} \overline{\rho}\,(E=0) \qquad &= \qquad \frac{1}{2(d-\nu)+1} \cdot \left|\frac{\Delta k}{\Delta E}\right| \\ &\approx \qquad \frac{1}{2\pi\,\gamma\,\sqrt{2}} \cdot \frac{2(d-\nu)+2}{2(d-\nu)+1} \\ &\approx \qquad \frac{1}{2\pi\,\gamma\,\sqrt{2}} \end{aligned} \tag{3.23}$$

With this result, the decay rate can be approximated by

$$\Gamma_k \;\approx\; \frac{1}{\gamma\,\sqrt{2}}\, S_k \;=\; \frac{1}{\gamma\,\sqrt{2}} \sum_{\nu,k'} 2^{\nu-1}\, M'_{k,\,k',\,\nu}. \tag{3.24}$$

To complete the expression, we need to evaluate the sum S_k. Expanding out $M'_{k,\,k',\,\nu}$ from Eq. 3.17, we find that we need to evaluate a triple sum over ν, j and k'.

$$S_k = \sum_{\nu=1}^{d} \sum_{k'=1}^{2(d-\nu)+1} 2^{\nu-1} M'_{k,\,k',\,\nu} \tag{3.25}$$

$$= \sum_{\nu=1}^{d} \sum_{k'=1}^{2(d-\nu)+1} \frac{2^\nu \sigma^2}{2(d+1)(d-\nu+1)} \left[2^{-d} \sin^2\left(\frac{k\,\pi}{2}\right) \sin^2\left(\frac{k'\pi}{2}\right) + \sum_{j=\nu}^{d-1} 2^{1-j} \sin^2\left(\frac{k\,\pi(j+1)}{2(d+1)}\right) \sin^2\left(\frac{k'\pi(j-\nu+1)}{2(d-\nu+1)}\right) \right]. \tag{3.26}$$

Since the sum over k' is independent of the other two, we will do this one first. The sum can be simplified if we convert the sines to complex exponential form, and then sum the resulting geometric series. The result for the non-central columns is elegant:

$$\sum_{k'=1}^{2(d-\nu)+1} \sin^2\left(\frac{k'\pi(j-\nu+1)}{2(d-\nu+1)}\right) = d-\nu+1. \tag{3.27}$$

It is easy enough to see that the result for the central column will be identical, since there the sine squared evaluates to 1 for odd k' and 0 for even k'. So we are left with

$$S_k = \sum_{\nu=1}^{d} \frac{2^\nu \sigma^2}{2(d+1)} \left[2^{-d} \sin^2\left(\frac{k\,\pi}{2}\right) + \sum_{j=\nu}^{d-1} 2^{1-j} \sin^2\left(\frac{k\,\pi(j+1)}{2(d+1)}\right) \right]. \tag{3.28}$$

Unfortunately, the factor of 2^{-j} in the sum over j prevents us from similarly simplifying the sum over j. Nonetheless, we can find a closed-form representation for it by a similar process:

$$\sum_{j=\nu}^{d-1} 2^{-j} \sin^2\left(\frac{k\,\pi(j+1)}{2(d+1)}\right) = 2^{-\nu} \left(1 + \frac{2\cos\left(\frac{k\,\pi\,(\nu+1)}{d+1}\right) - \cos\left(\frac{k\,\pi\,\nu}{d+1}\right)}{4\cos\left(\frac{k\,\pi}{d+1}\right) - 5} \right) - 2^{-d} \left(1 + \frac{2\cos(k\,\pi) - \cos\left(\frac{k\,\pi\,d}{d+1}\right)}{4\cos\left(\frac{k\,\pi}{d+1}\right) - 5} \right) \tag{3.29}$$

The final sum can be simplified further if we fix $E = 0$, or equivalently $k = d + 1$. In that case, the fractions on the right simplify to $(-1)^\nu/3$ and $(-1)^d/3$ respectively:

$$\sum_{j=\nu}^{d-1} 2^{-j} \sin^2\left(\frac{\pi(j+1)}{2}\right) = 2^{-\nu}\left(1 + \frac{(-1)^\nu}{3}\right) - 2^{-d}\left(1 + \frac{(-1)^d}{3}\right) \quad (3.30)$$

The sum over ν then yields

$$S_{E=0} \;=\; \frac{2\pi\,\sigma^2}{6(d+1)}\left(9 \cdot 2^{-d} + (-2)^{-d} + 6\,d - 10\right). \quad (3.31)$$

If we plot the matrix element sums S_k (Eq. 3.28) for varying k and d, we find that as d increases, the discrepancy for different choices of k in fact diminishes, and S_k converges to $S_{E=0}$ for all k (see Fig. 14). Finally, multiplying in the average density of states $\overline{\rho}$ from Eq. 3.23, we find an expression for the decay rate:

$$\Gamma_{E=0} \;\approx\; \frac{\sigma^2}{\gamma\sqrt{2}}\,\frac{\left(9 \cdot 2^{-d} + (-2)^{-d} + 6\,d - 10\right)}{6(d+1)}. \quad (3.32)$$

In the limit of large d, the first two terms in parentheses vanish, so if we define the constant $\Gamma_0 = \sigma^2/(\gamma\sqrt{2})$, then we have the $E = 0$ decay rate approximately given by

$$\Gamma_{E=0} \;\approx\; \frac{\sigma^2}{\gamma\sqrt{2}}\left(1 - \frac{8}{3(d+1)}\right) \;=\; \Gamma_0\left(1 - \frac{8}{3(d+1)}\right). \quad (3.33)$$

This convergence means that, for large depth graphs, we might expect the decay to simplify in character, becoming uniform. Furthermore, this happens to be the regime in which the Golden Rule is more applicable. The scaling of $\Gamma_{E=0}$ with d is shown in Fig. 15. Recall that the short-time decay rate we calculated was (from Eq. 3.14)

$$\Gamma_{j_0} \;\sim\; \sigma^2(1 - 1/N_{j_0}) \;\leq\; \sigma^2(1 - 2^{-d}). \quad (3.34)$$

Apart from a factor of $1/\gamma\sqrt{2}$, the rate bears a good resemblance to the approximate matrix element sum from Fermi's Golden Rule. Both rates depend on σ^2, and approach a limiting value for large d, although the rate of approach is slower for the Golden Rule result.

Although Fermi's Golden Rule yields no further results without a better method to evaluate the density of states, the calculation presented here still offers us a number of insights into how the column space probability decays.

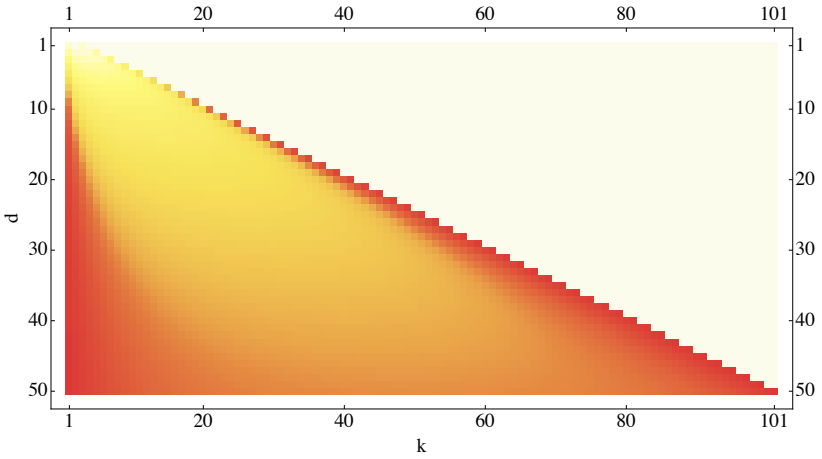

Figure 14: Plot of the matrix element sum S_k for the GT eigenstates $|\,\tilde{\psi}_k\,\rangle$. The discrepancy between the eigenvalues shrinks for increasing d, represented by a greater uniformity in the color of the plot.

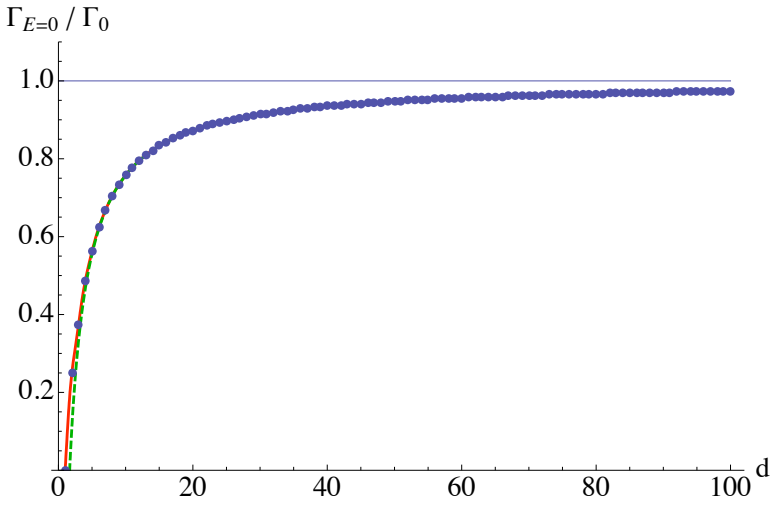

Figure 15: Convergence of $\Gamma_{E=0}$ for large d. The plot compares numerical values [blue points], the analytic expression in Eq. 3.32 *[solid red curve]* and the large d approximation $\Gamma'_{E=0}$ from Eq. 3.33 *[dashed green curve]*.

Local exponential decay

Armed with an understanding of how the decay rate for the column space probability depends on the walker's location, we can implement a fairly simple model of the decay, and compare this with simulations of the actual decay. For ease of computation, we will naturally choose to compute the walk evolution in the column space.

We know that the short-time decay model fails for time-scales on the order of the first hitting time, but it seems plausible that the decay rate might depend similarly on the walker's location for intermediate time decay. Furthermore, this is the exponential decay regime, in which the FGR model should also have some validity. The one important detail appearing in the FGR calculation, but not in the short-time decay calculation is the inverse dependence on γ, which we will include in the local decay model. This gives the decay rate the appropriate units. Therefore, we conjecture that the column space probability might decay as:

$$p_{col}(t) = p_0 \exp\left[-\frac{\sigma^2\, t}{\gamma}\left(1 - {N_j}^{-1}\right)\right], \tag{3.35}$$

at each column j. This column space decay is implemented by allowing the probability at each vertex $|\,\tilde{\mathrm{col}}\, j\,\rangle$ of the reduced graph to decay exponentially with the corresponding decay rate Γ_j. That is, we apply the mapping 2.7 to the system, representing each column of the graph as a single vertex on a line of length l. The evolution of the graph is then determined by the column space Hamiltonian, $\mathcal{H}_{\mathrm{col}}$. Implementing the column space decay is functionally equivalent to adding an imaginary diagonal component $\mathcal{H}_{\mathrm{decay}}$ to $\mathcal{H}_{\mathrm{col}}$, so the effective Hamiltonian ${\mathcal{H}_{\mathrm{col}}}'$ is defined by

$$\begin{aligned}
{\mathcal{H}_{\mathrm{col}}}' &= \mathcal{H}_{\mathrm{col}} + \mathcal{H}_{\mathrm{decay}} \\
&= \mathcal{H}_{\mathrm{col}} - i\sum_{j=0}^{l}\frac{\Gamma_j}{2}\,|\,\tilde{\mathrm{col}}\, j\,\rangle\langle\,\tilde{\mathrm{col}}\, j\,| \\
&= \mathcal{H}_{\mathrm{col}} - i\,\frac{\sigma^2}{2\,\gamma}\sum_{j=0}^{l}(1 - {N_j}^{-1})\,|\,\tilde{\mathrm{col}}\, j\,\rangle\langle\,\tilde{\mathrm{col}}\, j\,|
\end{aligned} \tag{3.36}$$

where the factor of $1/2$ is required since that Hamiltonian affects the probability amplitudes, which scale as the square root of the probability. The evolution defined by ${\mathcal{H}_{\mathrm{col}}}'$ is of course non-unitary, i.e. will not conserve probability – this is precisely what we are trying to model. This simplified model compares surprisingly well to simulations of the exact decay, as will be demonstrated in the following chapter.

3.5 Discussion

In this section, we have developed three basic models to describe the behavior of the column space probability under the influence of site disorder. The overall conclusion is that disorder introduces couplings between the eigenstates in the column space and those outside, with the effect of siphoning probability out of the column space. Since the two end nodes are in the column space, any probability leak out of the column space translates to a reduced hitting probability. Furthermore, Fermi's Golden Rule and the local decay model predict that the decay is exponential in character, the latter with with a position-dependent decay that grows as we approach the center of the graph, as well as with the size of the graph.

Based on the decay rate we derived, and the assumption of exponential decay, there are several predictions we can make at this point. First of all, we note that the density of eigenstates is highest at the center of the graph, and these furthermore have the most couplings to other eigenstates. So, we would expect that the decay eventually leads to a preponderance of probability in the center of the graph, as in the classical walk. Secondly, due to the exponential decay, the probability of reaching the exit node is indeed suppressed exponentially, particularly as the size of the graph increases.

However, there is an important distinction between this quantum decay and suppression of the hitting probability due to localization. Localization would imply that all wavefunctions are exponentially suppressed away from the entrance node. In fact, the suppression due to decay results from the buildup of probability outside the column space, which also removes probability from the entrance node. We therefore expect that for weak disorder, something resembling a quantum-to-classical transition will take place, with ballistic propagation and traversal of the full graph giving way to diffusion towards the center.

4 Simulations and results

4.1 Numerical methods

> *Very often, such a simplified model throws more light on the real workings of nature . . . It can be a disadvantage rather than an advantage to be able to compute or to measure too accurately, since often what one measures or computes is irrelevant in terms of mechanism. After all, the perfect computation simply reproduces* Nature*, does not explain her.*
>
> Phil Anderson, Nobel Lecture, 1977

Lacking a quantum computer on which to simulate the quantum walks in the presence and absence of disorder, we have instead compared our analytical results with simulations, studying the problem by numerically integrating the Schrödinger equation in MATLAB and FORTRAN. We first present several numerical strategies that we have employed to make the integration tractable.

Recall that the glued trees Hamiltonian is defined by the adjacency matrix of the graph (see Eq. 2.6). For the GT graph of degree d, there are $N_d \times N_d$ entries in the matrix, where $N_d = 3(2^d) - 2$. Exponentiating a matrix of this size is a non-trivial computation. Fortunately, however, for a given choice of d, the GT graph only has $4(2^d-1)$ edges, and thus the Hamiltonian has $8(2^d - 1)$ nonzero elements, all of which are ones. The matrix is therefore sparse, which allows us to simplify the calculation somewhat.

To approximate the matrix exponentiation, we apply a second-order splitting or symmetric product formula method, as described by De Raedt and Richardson [DR87, Ric91]. This scheme works by first breaking up the Hamiltonian into diagonal and off-diagonal terms,

$$\begin{aligned} \mathcal{H} &= \mathcal{H}_{\text{diag}} + \mathcal{H}_{\text{off-diag}}, \\ &= \sum_j \mathcal{H}_{j,j} \,|\, j \,\rangle\langle\, j \,|\, + \sum_{j \neq k} \mathcal{H}_{j,k} \,|\, j \,\rangle\langle\, k \,|, \end{aligned} \tag{4.1}$$

and then decomposing the off-diagonal portion into a sum of two-site operators. The matrix exponential is then approximated using the Baker-Campbell-Hausdorff (BCH) formula, which states that the exponential of a sum of matrices $dt(X + Y)$ can be written as

$$e^{dt(X+Y)} = e^{dt\,X}\, e^{dt\,Y}\, e^{-\frac{dt^2}{2!}[X,Y]}\, e^{\frac{dt^3}{3!}(2[Y,X,Y]]+[X,[X,Y]])} \ldots \tag{4.2}$$

In essence, we apply a set of matrix rotations pairwise to components of the wavefunction that are connected by a bond. That is, we express the off-diagonal Hamiltonian as the sum

$$\mathcal{H}_{\text{off-diag}} = \sum_{j<k} \mathcal{H}_{j,k}\, R^{(j,k)}, \tag{4.3}$$

with the operators $R^{(j,k)}$ defined as follows:

$$R^{(j,k)} = \big(|\, j \,\rangle\langle\, k \,| + |\, k \,\rangle\langle\, j \,|\big). \tag{4.4}$$

Then, we have

$$\begin{aligned} T^{(j,k)}(dt) &= \exp\Big(-i\, dt\, R^{(j,k)}\Big) \\ &= \cos dt\, \big(|\, j \,\rangle\langle\, j \,| + |\, k \,\rangle\langle\, k \,|\big) - i \sin dt\, \big(|\, j \,\rangle\langle\, k \,| + |\, k \,\rangle\langle\, j \,|\big) \\ &\quad + \sum_{l \neq j,k} |\, l \,\rangle\langle\, l \,|. \end{aligned} \tag{4.5}$$

Using the BCH formula, the time evolution operator can thus be approximated by

$$\begin{aligned} \mathcal{U}_{dt} &= \exp(-i\, dt\ \mathcal{H}_{\text{off-diag}})\, \exp(-i\, dt\ \mathcal{H}_{\text{diag}}) \\ &\approx \left(\prod_{j<k} \mathcal{H}_{j,k}\ T^{(j,k)}(dt)\right) \Phi(dt), \end{aligned} \tag{4.6}$$

where $\Phi(dt)$ stands for the phase rotations,

$$\Phi(dt) = \prod_{l} e^{-i\, \mathcal{H}_{l,l}\, dt} |\, l \,\rangle\langle\, l \,|. \tag{4.7}$$

We can in fact improve the accuracy of the algorithm above to third order by symmetrization. That is, we apply the rotations halfway, then the phase rotations, and finally complete the rotations in reverse order:

$$\mathcal{U}_{dt} = \left(\prod_{j,k} \mathcal{H}_{j,k}\ T^{j,k}(dt/2)\right)\ \Phi(dt)\ \left(\prod_{j',k'} \mathcal{H}_{j,k}\ T^{(j',k')}(dt/2)\right), \tag{4.8}$$

where $j' = N_d - j$, and similarly $k' = N_d - k$.

For our purposes, there are two Hamiltonians we will deal with, splitting them up as in Eq. 4.1 and proceeding in the manner outlined above. The first is the vertex space Hamiltonian, including site disorder terms,

$$\mathcal{H}_{\text{ver}} \quad = \quad \mathcal{H}_0 \, + \, \mathcal{H}_s \quad = \quad \mathcal{H}_0 \, + \, \sum_{j=1}^{N_d} \epsilon_j \, | \, j \, \rangle \langle \, j \, | , \tag{4.9}$$

and the second is the non-unitary time-evolution from the local decay model,

$$\begin{aligned} \mathcal{H}_{\text{col}}{}' \quad &= \quad \mathcal{H}_{\text{col}} \, + \, \mathcal{H}_{\text{decay}} \\ &= \quad \mathcal{H}_{\text{col}} \, - i \, \frac{\sigma^2}{2 \, \gamma} \, \sum_{j=0}^{l} (1 - {N_j}^{-1}) \, | \, \tilde{\text{col}} \, j \, \rangle \langle \, \tilde{\text{col}} \, j \, | \end{aligned}$$

as defined in Eq. 3.36. Exponentiating the second term in each Hamiltonian gives the Φ term in Eq. 4.7. The factor of $(-i)$ in $\mathcal{H}_{\text{decay}}$ causes the exponential decay of the probability.

4.2 Numerical results

Using the methods outlined above, we can begin to test the results we found earlier. We will vary two parameters: the graph depth, d, and the maximum disorder strength ε. For a given depth graph, we compare the dynamics over a range of disorder values up to ε, averaging over a number of iterations, with the diagonal terms of the Hamiltonian $\mathcal{H}_{ii} = \epsilon_i$ taken from a uniform distribution in the range $|\epsilon_i| \leq \varepsilon$. The main results we will present are the simulated evolution of the hitting probability at the end node, p_{hit}, the column space probability, p_{col}, the average depth d_{avg} and the standard deviation of the walker's depth, σ_d.

The bulk of the results presented below are drawn from two data sets comprising 3800 individual simulations, broken down as follows:

1. The range of depths runs from $d = 5$ to 23.
2. The disorder range runs from $\varepsilon = 0$ to 0.9.
3. Each of the combinations of d and ε is averaged over ten iterations for which the disorder is randomized.
4. Simulations are run separately for site disorder and bond disorder.
5. The simulations are run up to a maximum time of $4t_{hit}$, in 2500 steps.

The hitting time t_{hit} is an approximate value for the time at which p_{hit} is maximized. A first approximation would be to choose $t_{hit} = t_0 = l/\omega$, since the walk propagates at the speed $\omega = 2\sqrt{2}\gamma$. By approximating the location of the Bessel function's peak, we find that a small correction term $t' = 1.0188(l/2)^{1/3}/\omega$ improves the result considerably. So we set

$$t_{hit} \;=\; t_0 + t' \;=\; \frac{l + 1.0188(l/2)^{1/3}}{\omega}. \tag{4.10}$$

4.2.1 Ideal evolution

As a first test for the validity of our numerical results, we compare the results of our disorder-free simulations with the analytical results derived in Chapter 1. That is we set $\varepsilon = 0$, and simulate the walk on the graph G_d. As a reference case, we use $d = 15$.

Figure 16(a) shows the hitting probability at the end node, p_{hit} for t up to $4t_{hit}$, compared with the Bessel function solution (Eq. 2.19). The plots are in perfect agreement. The wavepacket first arrives at time $t = t_{hit}$, and returns, although with a slightly broader profile, two hitting times later. As anticipated, the probability is much more than exponentially small in the depth, and hence much greater than the classical hitting probability.

Second, Fig. 16(b) plots the average depth d_{avg}, showing once more the linear propagation across the graph, with reflections that sync with the arrivals at either root. Rather than the exact sum from Eq. 2.21, we show the continuum approximation, from Eq. 2.28. This plot closely resembles Fig. 10(b), and the agreement is once again good, although the approximation fails to capture the full magnitude of the d_{avg} oscillation.

Finally, Fig. 16(c) displays the standard deviation of the depth, σ_d. At first, the curve rises linearly, but dips periodically at each hitting time. This quantity σ_d measures the spreading of the wavepacket. Initially localized, the wavepacket spreads out as it propagates, due to the uncertainty in the momentum components. The coalescence marked by the dips is due to the reflection of the wavepackets at the ends of the graph. As time progresses, the wavepacket continues to spread, although we should be cautious not to extrapolate too far. This is the sort of behavior we plotted in Fig. 7.

While altogether unsurprising, it is a helpful validation that the numerical results bear out the analysis, even in the face of substantial approximations (e.g. the average depth calculation). These numerical plots are derived from a simulation on the vertex space of the graph, but if we use the column space Hamiltonian to implement the line-reduced evolution, we find the same results.

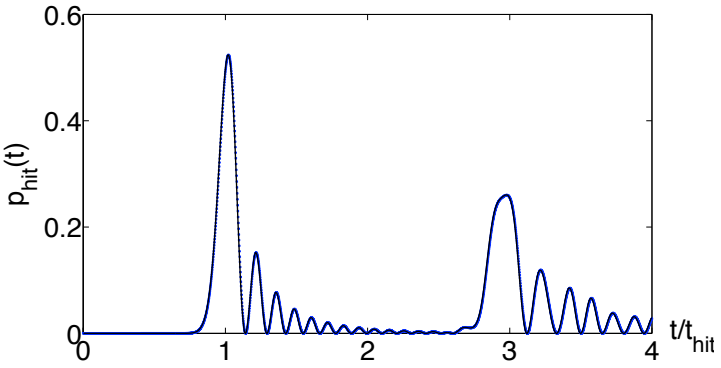

(a) $p_{hit}(t)$

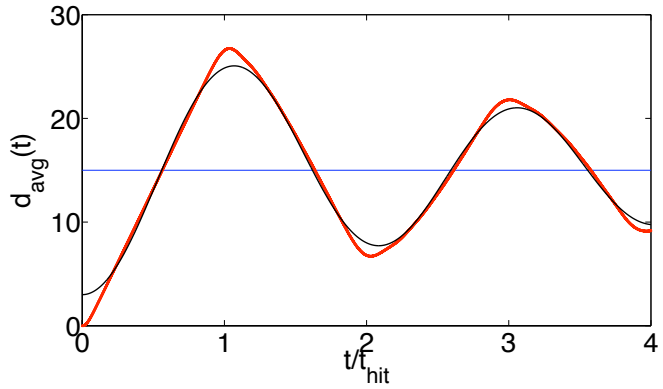

(b) $d_{avg}(t)$

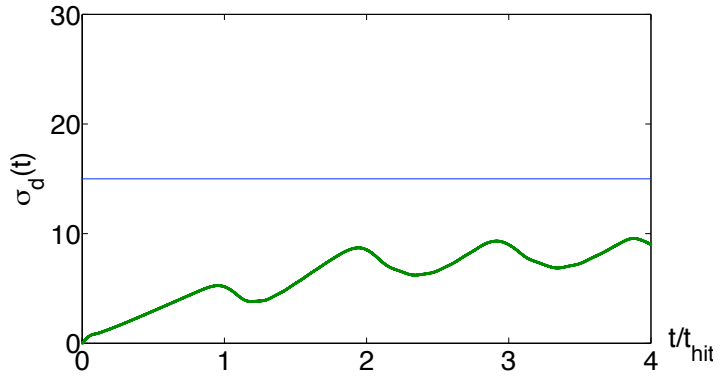

(c) $\sigma_d(t)$

Figure 16: Correspondence between simulation results *[colored points]* and analytical calculations *[black curves]* on the graph G_{15}. In the plot of d_{avg}, we plot the approximate result using the continuum limit, rather than the exact sum.

4.2.2 Disordered Evolution I: Column space decay

We have given arguments aplenty to predict a column space decay, and the numerical simulations undeniably bear out this result. The following two plots illustrate the global characteristics of the column space decay:

Fig. 17 shows the evolution of the column space probability p_{col} on a graph of depth 15. Plotting p_{col} on a semilog scale versus t and ε, we observe that p_{col} is proportional to $e^{-\varepsilon^2}$, and also decays roughly exponentially in time. For large disorder values, the probability of being in the column space has fallen by about one order of magnitude by the first hitting time, with similar consequences for the hitting probability. However, for weak disorder ($\varepsilon \lesssim 0.5$), there is still substantial probability in the column space up to four hitting times beyond the start of the evolution. So there is still a good chance of end-to-end propagation on the graph.

It is also interesting to follow the dependence of the decay on the degree of the graph, as shown in Fig. 18. The quadratic dependence of the decay rate on ε is again visible, but of more significance is its linear scaling with the depth of the graph. We have plotted p_{col} for $t = t_{hit}$, but recall that t_{hit} scales with the length of the graph ($l = 2d+1$) due to the linear propagation of the wavefunction. Therefore, it appears that the depth dependence is entirely due to the scaling of the hitting time, and not due to intrinsic differences between differently sized graphs. This result ties in well with the conclusions of the previous chapter, in which we found the decay rate to be nearly constant over most of the graph.

The next item on our agenda is to compare the simulated decay with the models we derived previously. We have already seen that the short-time decay of the column space probability seems to scale quadratically with time, in agreement with our perturbation theory result. Ideally, though, we would like to make more quantitative pronouncements about the scaling. However, the short-time decay from the initially localized state is essentially masked by the variation in position of the decay rate, and is thus difficult to observe. Starting the system in the central column state leads to a more uniform decay. The simulations agree with our calculations, but also reveal that the quadratic decay is valid only up to times on the order of $0.05t_{hit}$.

Although the Fermi's Golden Rule calculation is more sophisticated than the short-time decay, it yields only a single decay rate that varies for the different eigenstates, and is harder to apply to the case of a superposition over the eigenstates. So we proceed to compare the results of the local decay model with the exact simulation. The conclusions are heartening.

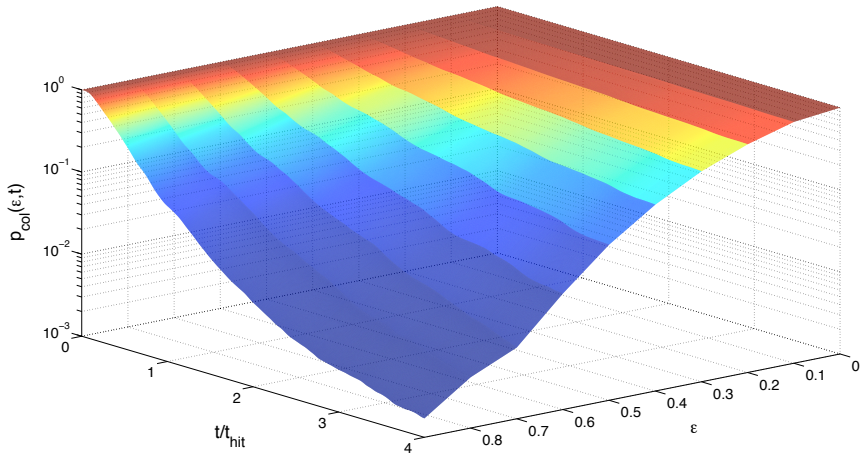

Figure 17: Semilog plot of $p_{col}(\varepsilon,\, t)$ for $d = 15$. The decay from the column space shows a definite Gaussian scaling with the disorder strength, and a time-dependence that is close to exponential, with some Gaussian character at short times.

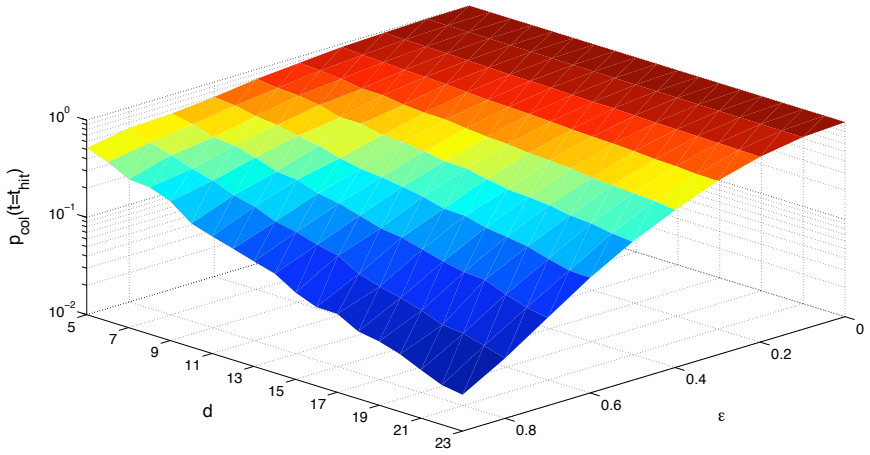

Figure 18: Semilog plot of $p_{col}(\varepsilon,\, d)$ for $t = t_{hit}$. The Gaussian dependence on the disorder strength is once again visible, as is an exponential dependence on the depth.

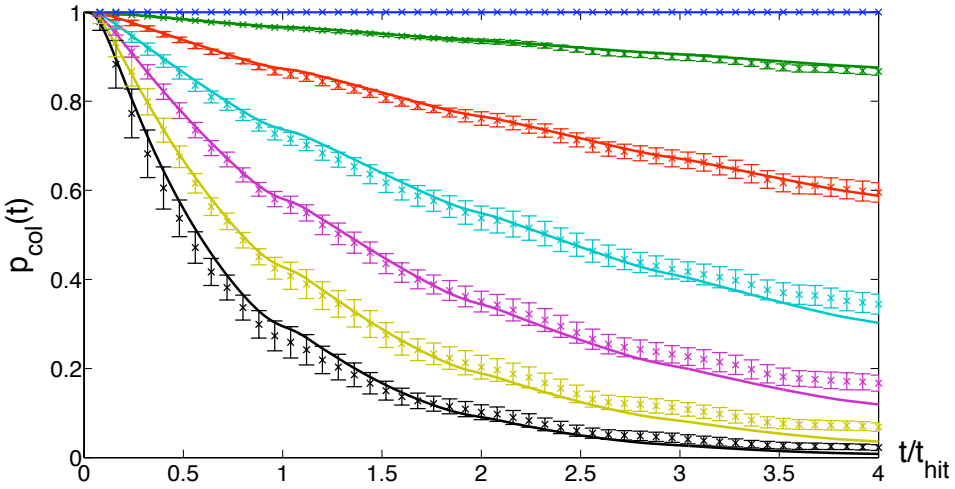

(a) $p_{col}(t)$

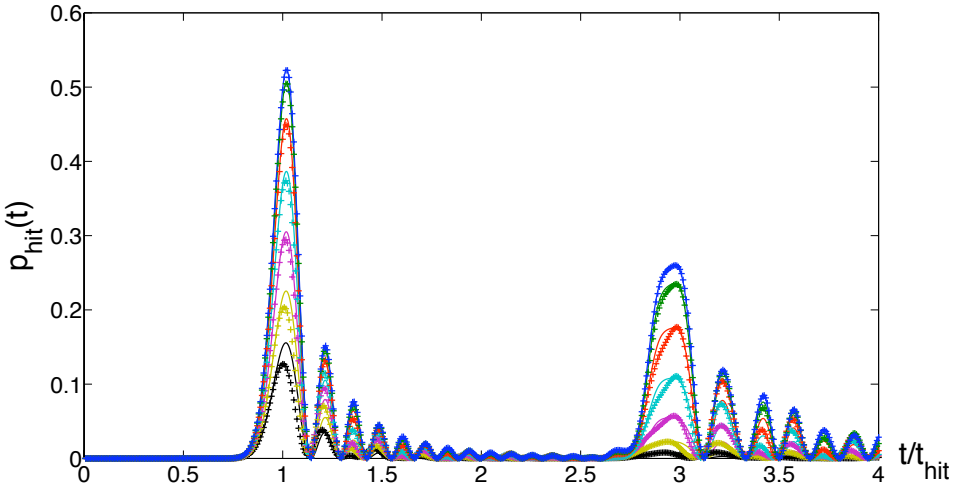

(b) $p_{hit}(t)$

Figure 19: Numerical values for $p_{col}(t)$ and $p_{hit}(t)$ on the graph G_{15}. The points represent the results of the numerical simulations, while the curves are the corresponding results from the local decay model. Disorder increases from 0 to 0.6, in steps of 0.1, with the zero disorder case shown by the topmost blue data set. For clarity, error bars are not shown in plot (b), however the local decay curves fall within one standard deviation of the plotted values.

Figure 19(a) shows the values of $p_{col}(t)$ up to four hitting times on the graph G_{15}, with disorder in the range $0 \leq \varepsilon \leq 0.6$. The remaining values of disorder show similar results, and have been omitted for clarity. Numerical results are shown by crosses, with the error bars given by the standard deviation of p_{col} over the ten averaged iterations. The curves are the corresponding values of p_{col} derived from the local decay model. The agreement is excellent, up to $t = 2t_{hit}$, although the model then begins to undershoot. In the local decay model, probability is lost permanently from the column space, and continues to decay indefinitely, whereas the decay levels off in the exact simulations. This breakdown of exponential decay may be due to the expected transition for systems with a lower bound energy [Kha58].

Especially impressive is the fact that the local decay model successfully reproduces fine features of the decay, such as the 'kinks' observed around integer multiples of t_{hit}. These correspond to times when the bulk of the probability is at either root of the graph, and our calculations in the previous chapter determined that the decay is reduced at those locations. Given that it can make detailed predictions of this sort, we are then motivated to examine whether or not it can reproduce the hitting probability from the vertex-space simulations. That is, assuming that the reduction in hitting probability is solely due to decay from the column space, the hitting probability ought to be reduced by the simple factor $p_{hit}(t) = p^0_{hit}\, p_{col}(t)$, with p^0_{hit} representing the hitting probability from the ideal Hamiltonian evolution. The comparison is plotted in Figure 19(b).

As with the column space probability, we find the local decay model to closely replicate the vertex-space simulations. In the magnitude of the oscillations, the agreement is good – it is primarily in the structure of the peaks that there are differences. Specifically, the peaks in the vertex-space simulations are slightly sharper, and shifted forwards at the first hitting time, although the maximum arrives later at the second hitting time ($t = 3t_{hit}$). For comparison, the classical hitting probability is estimated to be $1/N_d = 1.3 \times 10^{-5}$, so even with fairly strong disorder, where the magnitude of the perturbation terms is comparable to half the magnitude of the terms of the Hamiltonian, the quantum hitting probability is much higher.

To confirm that the hitting probability scales directly with the column space probability, we can plot the ratio of the two as a function of disorder strength and depth. Setting $t = t_{hit}$ is the most sensible choice, since this maximizes the hitting probability, and is a good reference point for the different depths. If we do this (see Fig. 20), we observe that the ratio is mostly independent of the disorder strength, below some limiting value (approximately $\varepsilon = 0.5$).

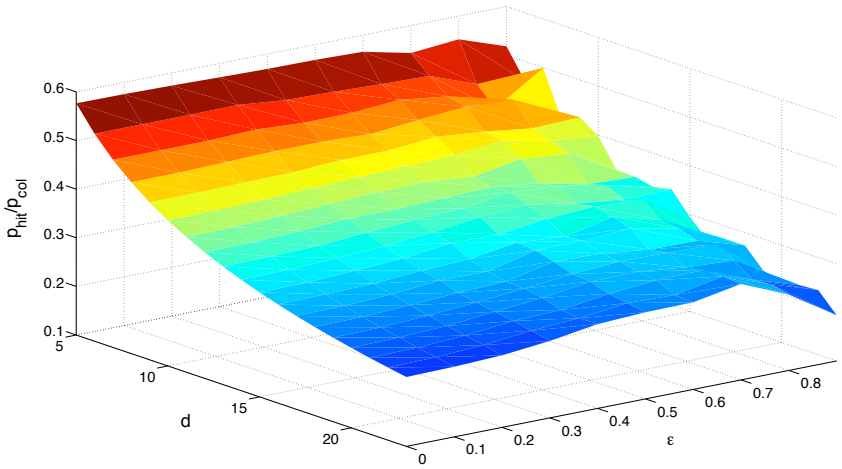

Figure 20: The ratio p_{hit}/p_{col} taken from the exact simulations, plotted at $t = t_{hit}$. For small disorder, this quantity is essentially independent of the disorder strength.

From these results, we conclude that, in the perturbative regime, the disorder does not substantially alter the behavior of the walk on the graph, except to cause a leak of the probability from column space states to states outside the column-space, which causes a diminished likelihood of reaching the end node (or returning to the start node). Hence, the local decay model provides a good method for determining the probability at either root.

4.2.3 Disordered Evolution II: A quantum-to-classical Transition?

We have now established the veracity of the column space decay, and demonstrated that, for varying levels of disorder, there remains some end-to-end propagation on the GT graph, as evidenced by the results for p_{hit}. The next question we would like to pose is whether we can characterize more accurately the degree of propagation achieved by the walker. To answer this question, we consider the effect of disorder on the average depth.

Before looking at the numerical results, let us reexamine the two cases for which we know the exact results for the evolution of d_{avg}. That is, recall that the quantum scenario results in an average depth that oscillates, with a slowly diminishing amplitude (similar to a damped oscillator in the un-

derdamped regime). The classical walker, however, approaches the center of the graph in a fashion that resembles an exponential decay. This resembles a critically damped oscillator (see Fig. 12(b)) Now, we might expect that adding disorder to the system disrupts the quantum mechanical features of the system in such a way that the characteristic evolution becomes closer to classical. In this case, we would expect the amplitude of the d_{avg} oscillations to decrease gradually, eventually turning into a similar exponential approach. The relevant plot is shown in Fig. 21.

In this figure, the evolution of the average depth very clearly transitions from oscillatory behavior to a decay towards the center of the graph ($d_{avg} = d = 15$). For all disorder strengths, the average depth initially grows linearly, the difference occurring when the walker reaches the center. The ideal walker simply keeps going, until it is reflected from the opposite end of the graph. As disorder increases, the walk progresses shorter distances from the center, and the average depth turns around earlier, rapidly coming to a halt at the center. So the quantum character of the walk is indeed lost.

For an explanation of this behavior, we need to recall two facts about the GT graph. Firstly, the density of eigenstates is much greater at the center of the graph (see Section 2.5), and hence when probability leaks out of the column space eigenstates, it must inevitably become more concentrated near the center.

Given the successes of the local decay model in predicting the decay of the column space probability and the hitting probability, we might wonder if it could be applied to replicate the results for the average depth as well. To do so, we need to account for the probability that has escaped from the column space. A naïve guess would be that all this probability winds up at the center of the graph. To test this, we run the local decay model, and compute the average depth using the probabilities in each column as provided by the simulation, but add a term $d_0(t) = d\,(1 - p_{col}(t))$ to the result, representing the remaining probability at the center.

This calculation of d_{ave} is shown in Fig. 22. The salient features of the vertex-space calculation are retained, with only one substantial difference. That is, for larger disorder values, the local decay model would seem to suggest an exponentially fast approach to the center of the graph, which is not a valid result. This is an artifact of the our assumption that all probability decays directly to the center of the graph; in truth, the non-column space probability will still take some time to propagate inwards. Nevertheless, this inaccuracy does not diminish the merit of the local decay model predictions in the case of weak disorder.

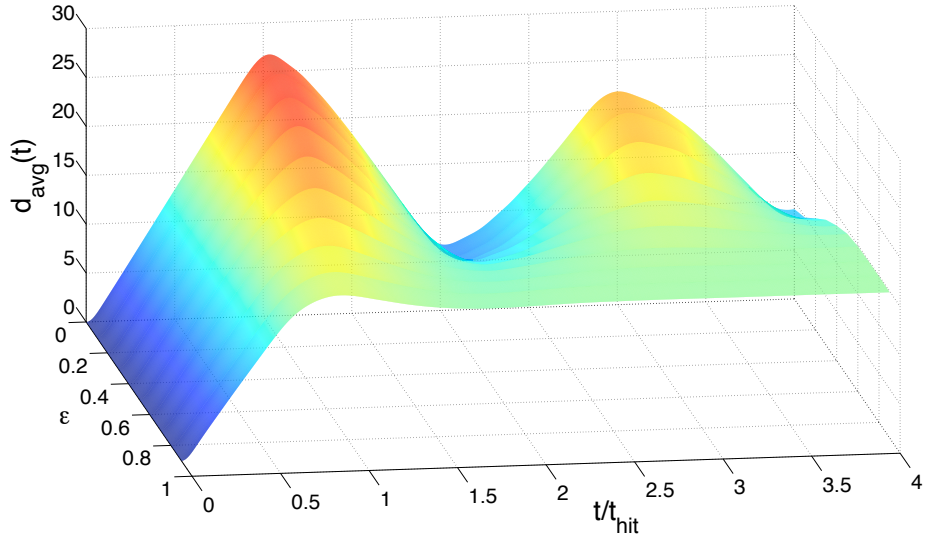

Figure 21: The average depth, $d_{avg}(t)$, plotted for $d = 15$, showing a transition from quantum ballistic propagation to classical diffusion.

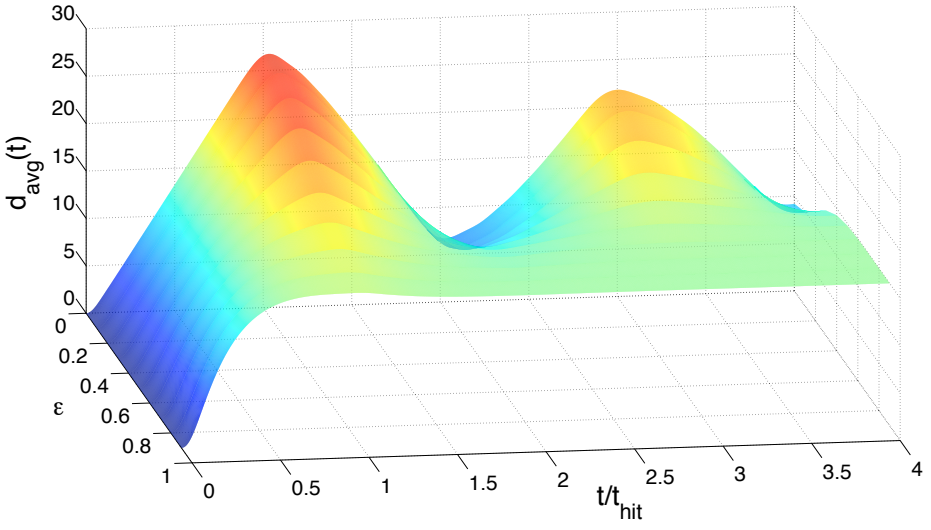

Figure 22: Approximation of the average depth reached by the walker, $d_{avg}(t)$, plotted for $d = 15$, calculated using the local decay model.

4.2.4 Disordered Evolution III: Whither localization?

All our results so far point to varying degrees of propagation, whether of the ballistic quantum sort, or transport more akin to classical diffusion. However, as mentioned earlier, analyses of the infinite Cayley tree predict the appearance of a localization transition for sufficiently large disorder. Insofar as the quantum walker ought to be unaware of the global structure of the graph in regions it has not yet reached, we expect similar results to hold for the Glued Trees: sufficiently large disorder should cause exponential localization of the walker near its starting point. That being said, the situation is complicated somewhat by the fact of the graphs' finite size. Particularly on smaller graphs, the localization length may be comparable to the size of the graph, in which case it will not significantly affect the dynamics.

Having set up the simulations for weak disorder, it is certainly not difficult to repeat the calculations in the context of large disorder. A paper by Girvin and Jonson calculates the Cayley tree localization transition to occur at $\varepsilon = 7.8$ in our units [JG79]. As we will see shortly, signs of localization appear before then; they already show up before $\varepsilon = 1.5$.

While this large discrepancy is somewhat disturbing, there are various possible explanations for the difference. Firstly, the precise location of the transition is hard to determine, in phenomenological terms. A system may demonstrate localization for some energies and not others. That is, there is a 'mobility edge' in the energy, which separates localized states from extended states. This situation complicates matters when the initial state is a superposition over the energy eigenstates, as is ours. It is therefore possible for a portion of the wavefunction to be localized, while the remainder continues to propagate. Furthermore, the quantities that we have been considering are not optimal as measures of localization: p_{hit} becomes negligible well before localization sets in, while p_{col} and d_{avg} do not offer direct pictures of the wavefunction. So it is hard at this stage to point to an exact number where we consider localization to have occurred.

That being said, plots of p_{col} and d_{avg} do have some insights to offer regarding the existence of localization. There are two harbingers of localization that we can point to: if the wavefunction becomes substantially localized at the starting position, then we expect *less* decay of the column space probability, since at the very least that amount of probability that remains at the start node stays in the column space permanently. The average depth reached also will hit some limiting value below d, i.e. the walker will not move to the center of the graph.

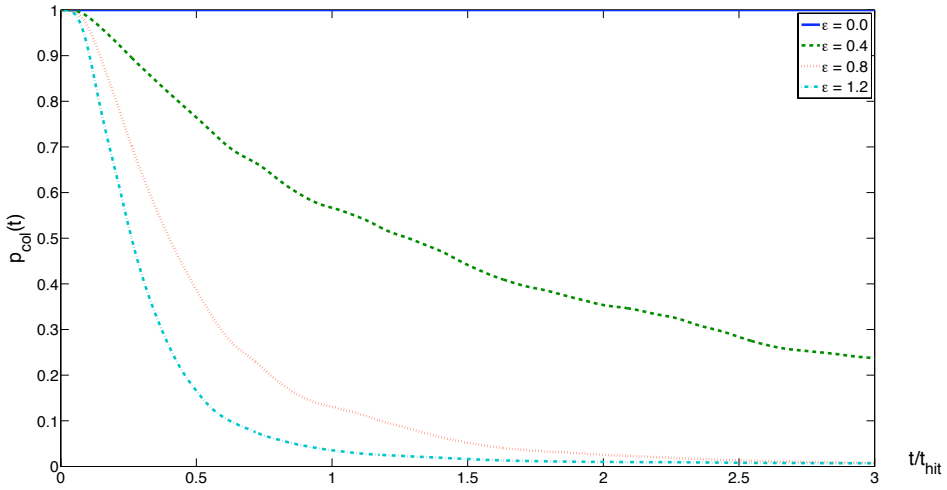

(a) Weak disorder ($0 \leq \varepsilon \leq 1.2$)

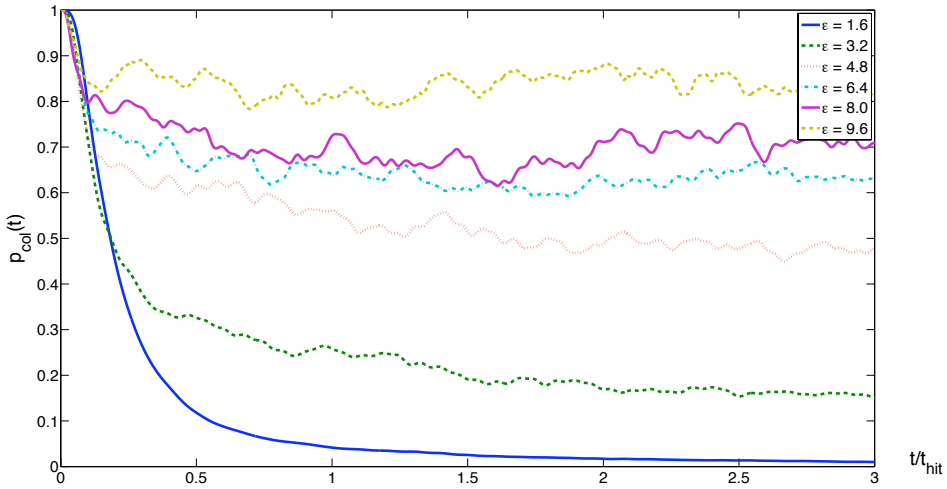

(b) Strong disorder ($1.6 \leq \varepsilon \leq 10$)

Figure 23: For weak disorder, we see column space decay as discussed previously, but for strong disorder ($\varepsilon > 1.5$), the decay of p_{col} is limited by the amount of probability trapped at the start node. (Plotted for G_{15})

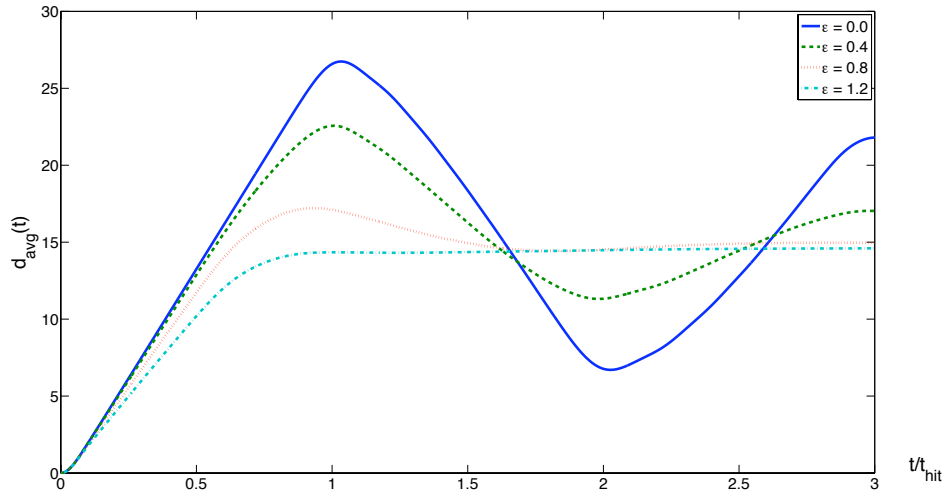

(a) Weak disorder ($0 \leq \varepsilon \leq 1.2$)

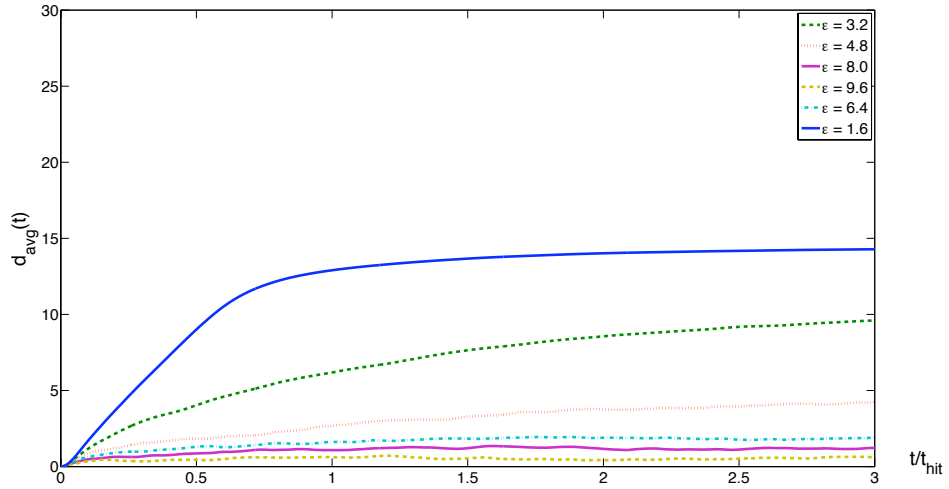

(b) Strong disorder ($1.6 \leq \varepsilon \leq 10$)

Figure 24: Weak disorder causes the transition from quantum to classical propagation, but strong disorder causes localization of the wavefunction, and the walker does not in fact reach the graph's center. (Plotted for G_{15})

On the previous two pages are plotted the column space probability and average depth at a range of disorder strengths, i.e with ε between 0 and 10. The boundary between 'weak disorder' and 'strong disorder' is between $\varepsilon = 1.2$ and $\varepsilon = 1.6$, which is when we begin to see a regeneration of the column space probability, as well as an average depth evolution that closely resembles the classical result. The contrast between the two regimes is stark, agreeing well with what we expect from a localization transition.

In the weak disorder regime, Fig. 23(a), we recognize the familiar column space decay, which occurs more and more rapidly with increasing disorder. Its character is essentially exponential, with very little probability remaining in the column space. However, the strong disorder plot is markedly different. In Fig 23(b), the initial decay profile is similar, with a short-term quadratic decay that quickly transitions to exponential decay. However, the decay eventually slows and halts at a finite value, which ought to nearly equal the probability localized at the start node. For $\varepsilon = 10$, it appears that as much as 80% of the wavefunction does not leave the origin!

The evolution of the average depth is shown in Fig. 24. In the weak disorder regime, the quantum-to-classical transition is clearly visible, whereas the walk in strong disorder appears to travel only part way across the graph, never assuming a form concentrated at the center. This difference in the degree of quantum transport arises from the difference in structure of the eigenstates of the Hamiltonian. For weak disorder, the perturbation does not substantially change the shape of the eigenstates; they remain extended over the graph. Once the disorder becomes sufficiently strong, however, the energy gap between neighboring sites becomes very large on average, and so the walker has little likelihood of hopping, making the eigenstates localized at individual sites.

We might well ask whether or not the localization transition is depth-dependent. Plotting the average depth or the column space probability at long times should give us an answer. The difference should be especially pronounced for times when the ideal walk is far from the center.

In Fig. 25, we plot the average depth d_{avg} for depths $d = 5$, 10, and 15, at $t = 3t_{hit}$. The average depth can be seen to converge for all three graphs, reaching a minimum value around $\varepsilon = 8$, in good agreement with the critical value computed by Girvin and Jonson [JG79]. Below this critical value, the eigenstates on the graph likely show varying degrees of localization, but upon reaching this transition, all the eigenstates become localized, regardless of the depth. At this point, the situation really is that of the Cayley tree, since the wavefunction can gain no information about the structure of the graph beyond the first few columns.

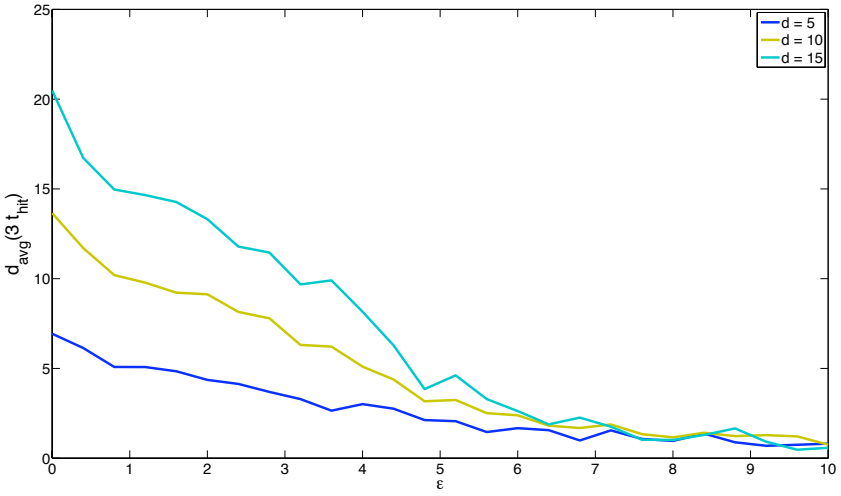

Figure 25: Plot of the average depth d_{avg} versus the disorder strength ε for depths $d = 5$, 15 and 20. The localization transition occurs around $\varepsilon = 8$.

Given the evidence for localization, we may well ask if this is not a vindication of the Keating results. The answer is an emphatic no! It is straightforward to simulate the walk in the column space, with diagonal disorder on the individual column-states, in which case we see localized behavior much earlier than in the vertex-space simulations. The evolution is given by the Hamiltonian from Eq. 1.15

$$\mathcal{H}_{\text{col}}{}' = \mathcal{H}_{\text{col}} + \sum_{j=0}^{2d} \epsilon_j |\,\tilde{\text{col}}\, j\,\rangle\langle\,\tilde{\text{col}}\, j\,|,$$

with ϵ_j drawn randomly from a uniform distribution over the range $-\varepsilon' \leq \epsilon_j \leq \varepsilon'$. In Fig. 26, we show plots of the average depth for simulations of this sort, using disorder strengths ranging from $0 \leq \varepsilon' \leq 0.9$. On the vertex-space, this would be solidly within the conductive regime, but the column space disorder simulations already show significant localization for $\varepsilon' \sim 0.4$, comparable to the vertex-space results for $\varepsilon = 4.0$. Hence, we can conclude that an implementation of diagonal disorder in the column space significantly overestimates the severity of the localization effects, and is an inadequate model for studying disorder on the graph.

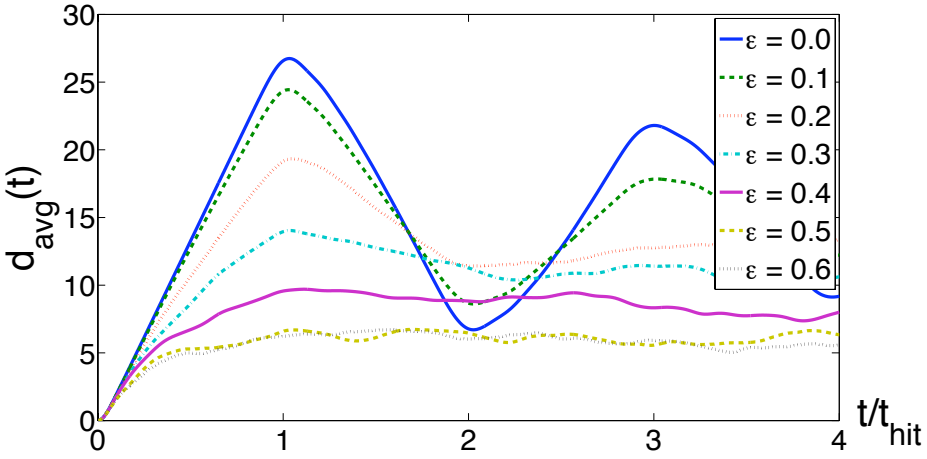

Figure 26: The average depth d_{avg} plotted for site disorder, implemented on the sites of the column space model. In this case, localization sets in considerably earlier.

4.3 Discussion

The results we have presented demonstrate three main characteristics of the quantum walk on the Glued Trees graphs in the presence of disorder. We have shown that the most significant effect of disorder is to couple the column space eigenstates to other states outside the column space, causing probability to be irretrievably lost from the column space via a process of exponential decay. Since the roots of the graph have support only on the column space eigenstates, this effect translates directly to reduced probability of arrival at the end node at the first and subsequent hitting times. In the perturbative regime, i.e. for weak disorder, we find that we can efficiently model the column space probability and the hitting probability by using a dynamical model incorporating local decay. Furthermore, for strong disorder, we observe evidence of a localization transition occurring at a critical value of the disorder strength.

A slightly different paradigm from the site disorder we have studied is bond disorder, i.e. modifications of the off-diagonal terms of the Hamiltonian. While the decay rate calculations are more complicated, particularly those for Fermi's Golden Rule, due to the couplings across column-states, we can make a simple estimate of how the effects of disorder should scale with the disorder strength. Since there are approximately three edges for each

vertex, and each of these edges will introduce phase-shifts for paths that traverse them, we might expect the bond disorder strength to have roughly three times the effect of the corresponding site disorder strength. That is, we estimate that the decay rates will be three times larger for bond disorder with the same disorder range. If we carry out the simulations, we find that this prediction indeed appears to be borne out: the decay is more severe, and localization begins to appear earlier.

It is downright simple to incorporate the bond disorder estimate into the local decay model, but the results are mixed. While the tripling of the decay rate matches up with the vertex-space calculations, we find that the timeframe in which the local decay model is valid shrinks by a corresponding factor. This is due to the essentially limitless decay of the model. In principle, for very large graphs this should be less of an issue since the fraction of probability that remains in the column space at large times is minuscule. That being said, this limitation of the model should not be brushed off.

Naturally, it would be an interesting problem to try to improve on the local decay model, in the hopes of extending the timeframe of validity without sacrificing the efficiency of the calculations. An obvious method is to account for return of the column space probability, or at the very least a modification of the decay rate at long times. If the former technique is to be used, however, the uncertainty about where the probability would return to necessitates a more complex treatment, involving the density matrix. Small returns might also be gained by improving the calculation of the average depth from the local decay model, for larger disorder values.

While much has been gained from studying small and intermediate degree graphs ($5 \leq d \leq 23$), our calculations suggest that the dynamics of decay might be simplified on much larger graphs ($d \geq 100$). Computing power sadly prevents us from attempting a vertex-space simulation of such large graphs, although groups with more power available would be encouraged to extend the calculations.

5 Conclusions

I think perhaps the most important problem is that we are trying to understand the fundamental workings of the universe via a language devised for telling one another when the best fruit is.

Sir Terry Pratchett

Our findings essentially indicate that quantum walks on the Glued Trees graph can be placed in three regimes based on the strength of disorder. For disorder terms that are small compared to the terms of the Hamiltonian, the walk remains essentially quantum-mechanical in character, showing linear propagation across the graph, although a growing proportion of the wavefunction becomes caught in the center of the graph. Once the disorder is comparable to the Hamiltonian, the dynamics become more classical in character, the wavefunction moving rapidly to the center of the graph, and subsequently remaining concentrated there. Once the diagonal terms of the Hamiltonian become dominant, the wavefunction becomes localized, and the walk becomes trapped at its starting point, with an exponentially small probability of being found further away.

The exponential decay of the column-space probability has mixed implications for the feasibility of implementing quantum-walk-based computation. The result of exponential decay appears to counteract the speedup, the most notable advantage of the quantum walk over the classical, putting the two paradigms on more equal footing. However, the fact that decay, and not localization, is the dominant source of the reduced hitting probability, means that the situation is less dire. First of all, the dependence of the decay is only quadratic in the size of the disorder, with the critical disorder strengths sufficiently large that it may be possible to design quantum circuits or other implementations with tolerable margins of error. Secondly, the propagation is largely a function of the column-space probability, so if techniques can be devised to retard the decay *a la* the 'watched pot' effect (e.g. by repeated measurements of the wavefunction's being in the column-space), this limitation may yet be overcome [SRM94].

In the spirit of scientific holism, one hopes that the techniques employed in the study of the Glued Trees walks can be extended to cover other systems. The obvious extensions are to graphs with similar symmetric structures, which enable the column-space analysis. These include the hypercube, dendrimer structures studied in the context of solar power, and of course the individual binary trees. We expect that decay from the column-space will

prove to be a similarly important aspect of the disordered walk dynamics for such systems.

There remain many open questions regarding the topics of the Glued Trees, column-space decay and disordered walks, and the work we have presented opens up several more. Likely the most important point is that the characterization of the walk in the presence of disorder is far from complete. While the local decay model serves very well for the timescales that are relevant to the problem of end-to-end propagation on moderately sized graphs, there is some doubt as to whether it continues to be valid in the limit of very large d, where simulation in the vertex-space is essentially unfeasible. Needless to say, extension of our simulations to much larger graphs ($d > 100$) would be a welcome comparison. It is possible that accounting for the return of probability to the column-space via the density matrix approach may be of use in improving the model. Also, the local decay model is effective at predicting the average behavior of the disordered graphs, but it is incapable of taking into account the specific variations in a single instance of disorder. This weakness is fortunately minor; for large graphs, the vertex-space is large enough that uncorrelated disorder will tend to average out over each column, and moreover an experimenter is unlikely to know the exact deviations in an experimental setup, so such a level of detail is probably unrealistic. In any case, simulations of single instances do not appear to deviate too significantly when compared with the averages.

Besides characterizing the effects of disorder on the Glued Trees, it would be interesting to examine the effects of other sorts of noise, such as decoherence of the wavefunction. While it is generally held that robustness against one sort of noise carries over to other kinds, it is also true that qualitiatively different effects arise from disorder and decoherence. The combined effects of different sorts of noise also form an interesting topic, albeit one further removed from quantum computation, in that the amounts of noise involved are considerably greater. In such contexts, localization may be more pronounced and more relevant, in which case a more in-depth analysis of the localization transition would be important. Likely, the Cayley tree results of Abou-Chacra et al. will be useful in such endeavors [ACTA73].

While discussing the application of Fermi's Golden Rule, we were forced to employ some less rigorous methods in approaching the density of states. This could in principle be improved upon, although as a tool, the Golden Rule is already an approximation, so it is uncertain what might be gained from such an investigation. Of greater interest, however, is the energy-dependence of the decay, which we have attempted to address only in passing. It is possible to study the amount of probability that decays into the

various eigenstates and sub-column-spaces, but due to the many couplings between eigenstates, the character of the decay is greatly complicated. The energy-dependence of the decay could also potentially add insights to the understanding of the localization transition and the mobility edge.

From the point of view of implementation, it is interesting to consider different schemata for encoding the Glued Trees walks. The issue of mapping general quantum walks to qubit Hamiltonians and back has been explored by Hines and Stamp [HS07b]. As an example, the structure of the d-dimensional hypercube is well-known to be encoded in the form of the collection of d-qubit strings, with edges connecting strings with Hamming distances of 1. Qubits are the most natural units to think of in terms of an experimental realization, so we would want to encode the GT graph in an n-qubit system. With $N_d = 3(2^d - 2)$ vertices, we will need at least $d + 2$ qubits, and at most N_d. The analysis above assumes an N_d qubit encoding (a.k.a. a unary encoding). Preliminary study suggests that encodings using the Hamming weight of $l = 2d + 1$ qubits to represent the current column-state or the minimal $d+2$ qubit encoding would be efficient to implement using quantum circuits, however much work remains to be done on this question.

Over and above the feasibility of the encodings lies the question of how robust the encoded systems will be against noise. Once again, the hypercube provides some hints. Previous studies have demonstrated that the maximally efficient qubit encoding, suffers more severely from decoherence and disorder than a'unary' encoding in which each qubit represents a vertex. Alagić and Russell's investigation of decoherence on the qubit-encoded hypercube determined that the hitting probability vanished for arbitrarily large graphs [AR05].

Strauch carried out a similar analysis, comparing the performance of the hypercube walk in two cases: dephasing between distinct faces of the hypercube (the 'subspace model of Alagić and Russell), versus dephasing between different vertices [Str09]. He found that for a fixed value of disorder or decoherence in the 'vertex model', the hitting probability approached a small but finite asymptotic limit as the graph size grew, in contrast to the subspace model. This result essentially ruled out localization. An argument in favor of the vertex model is that it assumes no knowledge of the graph structure, as ought to be the case in a physical realization. However, Hines has argued that the subspace model is more appropriate in the case of experimental realizations in qubit registers [HS07a]. The expectation is that similar results regarding the robustness of different encodings will hold for the Glued Trees, but analysis of this claim remains to be carried out.

References

[AALR79] E. Abrahams, P. W. Anderson, D. C. Licciardello, and T. V. Ramakrishnan, *Scaling theory of localization - absence of quantum diffusion in 2 dimensions*, Physical Review Letters **42** (1979), no. 10, 673–676.

[ACTA73] R. Abou-Chacra, D. J. Thouless, and P. W. Anderson, *A self-consistent theory of localization*, Journal of Physics C: Solid State Physics **6** (1973), no. 10, 1734–1752.

[ADZ93] Y. Aharonov, L. Davidovich, and N. Zagury, *Quantum random-walks*, Physical Review A **48** (1993), no. 2, 1687–1690.

[Amb03] Andris Ambainis, *Quantum walks and their algorithmic applications*, International Journal of Quantum Information **1** (2003), 507.

[And58] P. W. Anderson, *Absence of diffusion in certain random lattices*, Physical Review **109** (1958), no. 5, 1492–1505.

[AR05] G. Alagić and A. Russell, *Decoherence in quantum walks on the hypercube*, Physical Review A **72** (2005), no. 6, 062304.

[AS65] M. Abramowitz and I. A. Stegun, *Handbook of mathematical functions: with formulas, graphs, and mathematical tables*, Dover Publications, 1965.

[Bor63] R. E. Borland, *Nature of electronic states in disordered 1-dimensional systems*, Proceedings of the Royal Society of London Series A – Mathematical and Physical Sciences **274** (1963), no. AUG, 529–545.

[CCD+03] A.M. Childs, R. Cleve, E. Deotto, E. Farhi, S. Gutmann, and D.A. Spielman, *Exponential algorithmic speedup by quantum walk*, 2003, pp. 59 – 68.

[CFG02] A.M. Childs, E. Farhi, and S. Gutmann, *An example of the difference between quantum and classical random walks*, Quantum Information Processing **1** (2002), no. 35.

[CG04] A. M. Childs and J. Goldstone, *Spatial search by quantum walk*, Physical Review A **70** (2004), no. 2.

[Chi08] A.M. Childs, *On the relationship between continuous- and discrete-time quantum walk*, 2008.

[Coo71] Stephen Cook, *The complexity of theorem-proving procedures*, STOC '71: Proceedings of the third annual ACM symposium on Theory of Computing, ACM Press, 1971, pp. 151–158.

[DR87] Hans De Raedt, *Product formula algorithms for solving the time dependent schrdinger equation*, Computer Physics reports **7** (1987), no. 1, 1–72, doi: DOI: 10.1016/0167-7977(87)90002-5.

[EC71] E. N. Economou and M. H. Cohen, *Localization in one-dimensional disordered systems*, Physical Review B **4** (1971), no. 2, 396–404.

[FG98] Edward Farhi and Sam Gutmann, *Quantum computation and decision trees*, Physical Review A **58** (1998), no. 2, 915.

[FGR78] L. Fonda, G.C. Ghirardi, and A. Rimini, *Decay theory of unstable quantum systems*, Rep. Prog. Phys. **41** (1978), 588–631.

[Gam28] G. Gamow, *Zur quantentheorie des atomkernes*, Zeitschrift für Physik A **51** (1928), no. 3-4, 204–212.

[GJ80] S. M. Girvin and M. Jonson, *Dynamical electron-phonon interaction and conductivity in strongly disordered metal alloys*, Physical Review B **22** (1980), no. 8, 3583.

[Gro96] L. K. Grover, *A fast quantum mechanical algorithm for database search*, 1996, 237866 212-219.

[GS95] B. Gaveau and L. S. Schulman, *Limited quantum decay*, Journal of Physics A – Mathematical and General **28** (1995), no. 24, 7359–7374.

[HS07a] A. P. Hines and P. C. E. Stamp, *Decoherence in quantum walks and quantum computers*, 2007.

[HS07b] ———, *Quantum walks, quantum gates, and quantum computers*, Physical Review A (Atomic, Molecular, and Optical Physics) **75** (2007), no. 6, 062321–13.

[JG79] M. Jonson and S. M. Girvin, *Electron-phonon dynamics and transport anomalies in random metal alloys*, Physical Review Letters **43** (1979), no. 19, 1447.

[Kem03] J. Kempe, *Quantum random walks: an introductory overview*, Contemporary Physics **44** (2003), no. 4, 307–327.

[Ken07] V. Kendon, *Decoherence in quantum walks – a review*, Mathematical Structures in Comp. Sci. **17** (2007), no. 6, 1169–1220.

[Kha58] L. A. Khalfin, *Contribution to the decay theory of a quasi-stationary state*, J. Exptl. Theoret. Phys. (U.S.S.R.) **6** (1958), no. 33, 1053–1063.

[KLMW07] J. P. Keating, N. Linden, J. C. F. Matthews, and A. Winter, *Localization and its consequences for quantum walk algorithms and quantum communication*, Physical Review A (Atomic, Molecular, and Optical Physics) **76** (2007), no. 1, 012315–5.

[Lev73] L. A. Levin, *Universal search problems (in russian)*, Problemy Peredachi Informatsii **9** (1973), no. 3, 265–266.

[Pap91] C. H. Papadimitriou, *On selecting a satisfying truth assignment*, 32nd Annual Symp on Foundations of Computer Science (San Juan, Pr), IEEE, 1991, pp. 163–169.

[Pea05] K. Pearson, *The problem of the random walk*, Nature **75** (1905), no. 1865, 294.

[Ray05] J. Rayleigh, *Re: The problem of the random walk*, Nature **72** (1905), no. 1866, 318.

[Ric91] J. L. Richardson, *Visualizing quantum scattering on the cm-2 supercomputer*, Computer Physics Communications **63** (1991), no. 1-3, 84–94, doi: DOI: 10.1016/0010-4655(91)90240-L.

[Sch68] L. I. Schiff, *Quantum mechanics*, 3rd ed., McGraw-Hill, New York, 1968.

[Sch86] S. S. Schweber, *Feynman and the visualization of space-time processes*, Reviews of Modern Physics **58** (1986), no. 2, 449.

[SKW03] N. Shenvi, J. Kempe, and K. B. Whaley, *Quantum random-walk search algorithm*, Physical Review A **67** (2003), no. 5, 11.

[SRM94] L. S. Schulman, A. Ranfagni, and D. Mugnai, *Characteristic scales for dominated time evolution*, Physica Scripta **49** (1994), no. 5, 536–542.

[Str06] F. W. Strauch, *Connecting the discrete- and continuous-time quantum walks*, Physical Review A **74** (2006), no. 3, 4.

[Str09] ———, *Reexamination of decoherence in quantum walks on the hypercube*, Physical Review A (Atomic, Molecular, and Optical Physics) **79** (2009), no. 3, 032319–8.

[Zal07] A. Zaliznyak, *Levy flights and scale invariance in stochastic searches*, 2007.